nature portfolio

# Peer Review File

# Modeling NK-cell lymphoma in mice reveals its cell-of-origin and microenvironmental changes and identifies therapeutic targets

Corresponding Author: Professor Keisuke Kataoka

Parts of this Peer Review File have been redacted as indicated to maintain the confidentiality of unpublished data.

**This file contains all reviewer reports in order by version, followed by all author rebuttals in order by version.**

Version 0:

Reviewer comments:

Reviewer #1

(Remarks to the Author)

The manuscript by Koya et al. underscores the critical challenge posed by the absence of a genetically engineered mouse model that can faithfully replicate the genetic events observed in human ENKTCL, thus impeding the understanding of tumorigenesis and exploring therapeutic targets of such cancer type. For this aim, the authors established a mouse model harboring NK-cell-specific Trp53 deletion. They showed that Trp53 deficiency could induce NK-cell neoplasms primarily involving the salivary glands (SG), and the expression of EBV-encode LMP1 accelerated such lymphomagenesis. Regarding the changes in the tumor microenvironment during this process, they highlighted the interaction between myeloid cells, particularly cDC cells and NK tumor cells, via Cxcl6-Cxcr6. At last, they pointed out that KLRG1 in tumor cells could be a potential therapeutic target in ENKTCL. Overall, the mouse model established in this model could contribute to studying EBV-related ENKTCL. However, the manuscript shows a lack of mechanistic insights. Although the authors tried to dissect the mechanisms using scRNA-seq, the data are not well analyzed, interpenetrated, and validated. Here are my major concerns.

Regarding the single-cell analyses:
1. The sub-clustering analysis failed to distinguish immune subsets effectively. For instance, the Tregs identified by the authors comprised nearly half of the recovered CD4 T cells yet displayed a surprisingly low expression of Foxp3, a key marker for Tregs. This inconsistency could raise the mis-annotation of cell subsets, thereby undermining the reliability of the subsequent conclusions obtained in this study. Another example is the cDC cell population, which has been documented to divide into different cell subsets, such as cDC1 and cDC2. The author only provided the global cluster of such cells.

2. This study used scRNA-seq to demonstrate the changes in myeloid cell types. The statistical analyses are needed to strengthen their findings. For ligand-receptor pairs and therapeutic targets highlighted, they should provide additional validation, such as flow cytometry analyses from their mouse models and clinical samples.

3. The authors observed elevated responses and outgoing signals in myeloid cells within tumors, suggesting a coordinated response in these cell types. Given the high abundance of these cells in the samples, further analyses are needed to determine whether specific subpopulations within these broader categories are the primary drivers of the cellular processes and communicating signals highlighted in this study.

4. The pro-tumor role of interactions between cDC and tumor cells via Cxcl16-Cxcr6 in this tumor model is not convincing. Specifically, there are comparable interactions between monocytes/macrophages and CD8 Tem cells. Additionally, Cxcr6 is critical for tumor control for CD8 cytotoxic T cells in previous studies (Pilato Cell, 2021). The authors simply described the signals in tumor cells but ignored those on CD8 T cells, which could also be the anti-tumor ones.

Other major concerns:
1. In lines 112-115, the diagnostic foundation for a lethal hematopoietic neoplasm involving the SG should extend beyond

reliance on complete blood count and macroscopic evaluation. A more robust diagnostic approach is essential to conclusively assert that the hematopoietic neoplasm in NK-cell-specific Trp53 conditional knockout mice has manifested.

Furthermore, additional elucidation on the ENKTCL model within the GEMM is needed. A more comprehensive account of the developmental processes of ENKTCL in GEMM is necessary, accompanied by a detailed explanation of the methodologies employed to confirm the occurrence of ENKTCL in the mice. The authors should also compare the mutation signatures between mouse models and those from patients to validate their models further.

2. While the authors noted an upregulation of both Cxcl9-Cxcr3 and Cxcl16-Cxcr6 signaling in Trp53-/-LMP1+ tumor cells compared to Trp53-/- tumor cells, the manuscript predominantly delves into the investigation of Cxcl16-Cxcr6 signaling. The specific details or analyses pertaining to Cxcl9-Cxcr3 signaling are not as thoroughly explored in the provided information. The author should clarify their investigation of Cxcl9-Cxcr3 signaling, providing a detailed examination of its role and impact within the context of Trp53-/-LMP1+ tumor cells.

3. In lines 275-281, the authors mentioned that Lin-KLRG1+ cells could develop into NK-cell tumors upon transplantation into secondary recipients, implying that KLRG1 expression can potentially identify tumor-initiating cells. However, there is a lack of discernible differences in the proportion of Lin-KLRG1+ cells between WT, Trp53-/-, and Trp53-/-LMP1+ during the pre-tumor stage.

The data presented suggests a plausible association between KLRG1 expression and tumor formation, but the conclusion that KLRG1 marks tumor-initiating cells requires additional substantiation. The authors should provide more evidence to support their claims regarding the role of KLRG1 in tumor initiation. This will strengthen the overall interpretation and validity of the findings related to KLRG1 expression in the context of tumorigenesis.

Minor points:
1. In Fig. 1e and Fig. 3c, histological examination for WT mice should be provided.
2. In Fig. 1g, the proportion of Lin- cells between WT and Trp53-/- mice in SG did not show statistical significance. It seems to be a decreasing tendency in Trp53-/-. The author should explain the different alterations of such cells in SG and SP from the Trp53-/- models.
3. In Fig. 3c, the authors should summarize the H&E staining data and perform statistical analysis.
4. In Fig.4, more detailed analyses are needed to support their conclusion.
5. In Fig. 5, further experiments are needed to confirm that Trp53-/-LMP1+ tumors secrete more IFNγ, such as FACS or ELISA assay.

Reviewer #2

(Remarks to the Author)
Excellent manuscript outlining the role Trp53 and EBV-encoded latent membrane protein 1 expression NK-cell lymphomagenesis in mice and potential for KLRG1 targeting as a therapy

I think the manuscript is very solid as is

Congrats to the authors

Reviewer #3

(Remarks to the Author)
The manuscript by Koya et al. details a murine model of extranodal NK cell lymphoma, focused on the overexpression of TP53 in murine NK cells specifically. The authors demonstrated that knocking out Trp53 in all Ncr1 positive cells leads to expansion of NK cell tumors that are subsequently transplantable. When Lmp1 was overexpressed in the presence of Trp53 knockout, the tumors were more aggressive, yet maintained a similar pattern. Finally, use of a depleting antibody against the NK cell maturation marker, KLRG1, led to improved overall survival in the mice. Overall the studies were robust and provided extensive transcriptomic analysis of the murine model of Trp53 knockout, as well as additional ENKTCL human samples.

There are some remaining questions about the biology behind the model.

• First, human ENKTCL is defined by the presence of EBV within the NK cells, so the abundance of TP53 mutations in patients occurs in the backdrop of EBV-infection. How do the Trp53 KO cells compare to EBV-infected TP53 mutated NK cells in patients?
• Is the hypermethylation observed in EBV+ malignancies preserved in this model?
• The model of Trp53 KO with Lmp1 overexpression suggests there is more heterogeneity of KLRG1 expression as compared to the Trp53 KO alone-is there a difference in clonal expansion?
• Additional immunophenotyping of the model demonstrating protein expression of NK-associated TFs and maturation markers would further classify the stage of NK cells in the model
• For translational relevance, do human TP53 mutated ENKTL samples have elevated protein expression of KLRG1, and is

this uniformly expressed like the mouse model or variable?
• Several prior studies have identified human tissue-resident NK cells as the cell of origin of extranodal NK lymphoma-comparing the findings in this murine model with recently published human data would be useful
• Support demonstrating relevance of myeloid infiltration with human NK lymphomas would support additional relevancy of the model
• The impact of KLRG1 depletion was modest in the model with Lmp1 overexpression-were there additional targets uncovered unique to this model which may correlate most closely with human NK lymphoma?

Version 1:

Reviewer comments:

Reviewer #1

(Remarks to the Author)
The authors have provided detailed explanations and performed additional experiments, effectively addressing my previous concerns. Regarding the analyses, the manuscript has been improved to achieve a higher resolution in identifying cell populations. However, the selection of markers for several populations presented in the figures remains suboptimal, compromising the reliability of their annotations. For instance, Cd209a and Cd300a would be more appropriate markers for cDC2, Ifng and Tbx21 for CD4 Th1 cells, and Havcr2, Lag3, Entpd1, and Tox for Tex cells. The authors should conduct a thorough investigation to identify and utilize more appropriate markers for these cell populations.

Additionally, the use of binomial-based tests for enrichment analysis is not optimal for robust comparisons between groups. Given that changes in cell abundance are a key finding of this study, it is imperative to include biological replicates and apply t-tests or Wilcoxon tests to strengthen the evidence supporting these changes.

Overall, the manuscript is much improved.

Reviewer #3

(Remarks to the Author)
The authors have provided additional data demonstrating comparable pathway activation between the TP53 mutated ENKTL mouse model and human ENKTL, which enhances the translational potential. There were also some differences observed as expected in the absence of EBV, such as a lack of hypermethylation in the tumor cells from the mouse. There are a few outstanding questions and clarifications that would help in the interpretation of the findings.

• The definition of the cell of origin is still somewhat unclear-the authors state that the cell of origin for the murine lymphoma must be an immature NK cell as it is CD122+/Lin-, however this population was later described to also harbor T cell and non-NK ILC potential. In addition, these cells were shown to express Tbet and Eomes, and not NK1.1, yet Tbet and Eomes would normally be expressed after/coinciding with NK1.1 expression in the NK cell lineage. The other antigens evaluated are likewise not specific to NK cells, and there are a mix of immature and mature markers expressed (including KLRG1) which point away from a precursor population. The NK cell development pathway is well characterized in mouse, with numerous reports utilizing reporter mice and/or genetic depletion models in the last few years, and comparing the transcriptional and immunophenotypic findings to what is already established in the field for development would be helpful to defining this population as the current description alone is insufficient to define an NK-restricted precursor population.
• The authors also stated this is the first report defining the cell of origin being a tissue residency NK cell, however recent reports on human NK lymphoma have already established the association between tissue resident NK cell phenotypes and categories of NK lymphoma (reference #13). Discussing the findings in this model with the established human data would increase the relevancy/translation. In addition, CD49a alone does not demonstrate tissue residency as CD49a is well established as being upregulated on activated NK cells.
• The new Cibersort data from primary ENKTL did not specify the mutational profile of those samples-was there myeloid infiltration observed in TP53 mutated human ENKTL? It was also curious that only a low proportion of NK cell infiltration was shown for some of the sequencing samples-wouldn't the vast majority of the tumor samples be associated with an NK cell transcriptional profile if the sample was primarily of tumor origin? Was there any normal adjacent tissue or control tissue that was analyzed in the same manner to provide background immune cell composition?
• There is an overall lack of controls being pictured in the new data (and explanation for what is being shown). In the flow histogram plots for example, is that an isotype control being shown, or an internal negative? How do these levels compare to those found in stages of murine NK cells (for the transcription factor data)? Please describe in more detail.
• For histology, please provide normal tissue staining to demonstrate specificity of the antibody staining being evaluated. H+E was provided for mouse, but the antibody staining should likewise have controls.
• Flow dot plots should be shown for the new IFNy data in addition to bar graph (along with isotype controls)

Version 2:

Reviewer comments:

Reviewer #1

(Remarks to the Author)
The manuscript has been improved, and the authors have addressed all my concerns. I have no further comments.

Reviewer #3

(Remarks to the Author)
The authors have addressed the question of origin interpretation and placed their work in the context of the field to a higher degree-including additional studies and enhanced transperancy. In addition they have added additional controls and support for their conclusions. No further revisions are requested.

**Response to Reviewer Comments**

**NCOMMS-24-12212-T**
**Modeling NK-cell lymphoma in mice reveals its cell-of-origin, microenvironmental changes, and therapeutic targets.**

We thank the reviewers for their insightful comments and suggestions, which have helped to significantly improve our manuscript. We believe that our new data and discussion address all of the reviewer's suggestions. Each of the reviewers' specific comments are addressed in full below.

**Reviewer #1 (Remarks to the Author):**
The manuscript by Koya et al. underscores the critical challenge posed by the absence of a genetically engineered mouse model that can faithfully replicate the genetic events observed in human ENKTCL, thus impeding the understanding of tumorigenesis and exploring therapeutic targets of such cancer type. For this aim, the authors established a mouse model harboring NK-cell-specific Trp53 deletion. They showed that Trp53 deficiency could induce NK-cell neoplasms primarily involving the salivary glands (SG), and the expression of EBV-encode LMP1 accelerated such lymphomagenesis. Regarding the changes in the tumor microenvironment during this process, they highlighted the interaction between myeloid cells, particularly cDC cells and NK tumor cells, via Cxcl6-Cxcr6. At last, they pointed out that KLRG1 in tumor cells could be a potential therapeutic target in ENKTCL. Overall, the mouse model established in this model could contribute to studying EBV-related ENKTCL. However, the manuscript shows a lack of mechanistic insights. Although the authors tried to dissect the mechanisms using scRNA-seq, the data are not well analyzed, interpenetrated, and validated.

We appreciate the reviewer for the time and expertise in reviewing the manuscript and are very pleased that he/she considers that our mouse models could contribute to studying EBV-related ENKTCL. As described in detail below (in #1-1, -2, and -3), we re-analyzed scRNA-seq data to address the reviewer's concerns.

**#1-1**
The sub-clustering analysis failed to distinguish immune subsets effectively. For instance, the Tregs identified by the authors comprised nearly half of the recovered CD4 T cells yet displayed a surprisingly low expression of Foxp3, a key marker for Tregs. This inconsistency could raise the mis-annotation of cell subsets, thereby

undermining the reliability of the subsequent conclusions obtained in this study. Another example is the cDC cell population, which has been documented to divide into different cell subsets, such as cDC1 and cDC2. The author only provided the global cluster of such cells.

To address the reviewer's comments, we performed clustering and subclustering of $CD4^+$ T, $CD8^+$ T, NK, B, and myeloid cell clusters again with a higher resolution. We identified 3 $CD4^+$ T, 5 $CD8^+$ T, 1 NK, 3 B, and 7 myeloid subclusters. Specifically, $CD4^+$ T-cell subclusters included naive, effector memory (EM), and Treg subclusters. The Treg subcluster accounted for 21.6% of $CD4^+$ T cells and showed clear expressions of Treg markers, including *Foxp3* (**Supplementary Fig. 5i,j**). $CD8^+$ T-cell subclusters included naive, EM, central memory (CM), resident memory (RM), and exhausted (EX) subclusters (**Supplementary Fig. 5i,j**). In myeloid subclusters, we successfully separated conventional dendritic cell (cDC) into cDC1 and cDC2 and identified a new subcluster representing mature DC enriched in immunoregulatory molecules (mregDC), which was recently discovered in scRNA-seq of lung cancers and is characterized by co-expression of immunoregulatory genes (*Cd274* and *Cd200*) and maturation genes (*Cd40* and *Ccr7*) (**Fig. 5a and Supplementary Fig. 6a**). As a result, myeloid subclusters included monocyte (Mono), myeloid-derived suppressor cell (MDSC), macrophage (Macro), cDC1, cDC2, plasmacytoid DC (pDC), and mregDC. Therefore, we believe that our new analysis effectively distinguishes immune subclusters. Using these new subclusters, we re-performed all downstream analyses and obtained similar results. Therefore, we have added the explanation and the data in **Results**, **Methods**, **Fig. 5a**, and **Supplementary Fig. 5i,j, and 6a** in the revised manuscript as follows.

**Results**

**(Page 10, line 244)**

To further characterize immune cell clusters, we performed subclustering, which identified 3 $CD4^+$ T-cell (naive, effector/memory [EM], and Treg), 5 $CD8^+$ T-cell (naive, central/memory [CM], EM, resident/memory [RM], and exhausted [EX]), and 3 B-cell (immature, mature, and plasmablasts) subclusters (**Supplementary Fig. 5i,j and Supplementary Table 8**). Both *Trp53*$^{-/-}$ and *Trp53*$^{-/-}$*LMP1*$^+$ tumors showed decreased naive T cells, whereas $CD8^+$ T EX cells were increased in the extranodal tissues from *Trp53*$^{-/-}$*LMP1*$^+$ tumors (**Fig. 4c and Supplementary Table 9**), suggesting enhanced T-cell exhaustion in *Trp53*$^{-/-}$*LMP1*$^+$ tumors.

**(Page 11, line 255)**

The myeloid subclusters included monocyte (Mono), macrophage (Macro), type 1 and 2 conventional dendritic cell (cDC1 and cDC2), plasmacytoid DC (pDC), mature DC enriched in immunoregulatory molecules (mregDC), and myeloid-derived suppressor cell (MDSC) (**Fig. 5a, Supplementary Fig. 6a, and Supplementary Table 8**). A higher proportion of Mono and cDC1 were observed in *Trp53*$^{-/-}$*LMP1*$^{+}$ tumors from both the extranodal tissues and SP, whereas MDSC was strongly enriched in the SP (**Fig. 5b and Supplementary Table 9**). By contrast, Macro, pDC, and mregDC were decreased in the SP from *Trp53*$^{-/-}$*LMP1*$^{+}$ tumors.

**Fig. 5a**

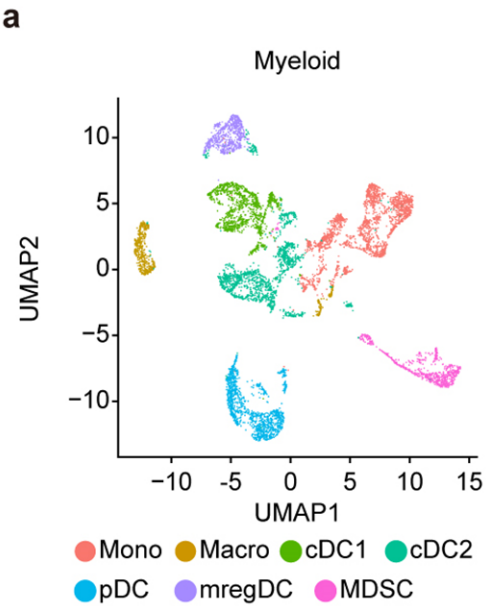


**a,** UMAP plot of subclustering of myeloid cells.

## Supplementary Fig. 6a

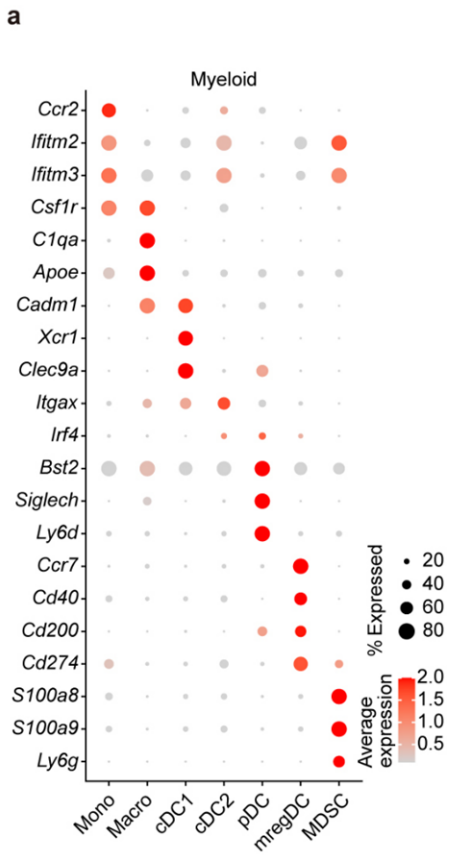


**a,** Bubble plot of representative mRNA markers for each myeloid cell subcluster.

## Supplementary Fig. 5i

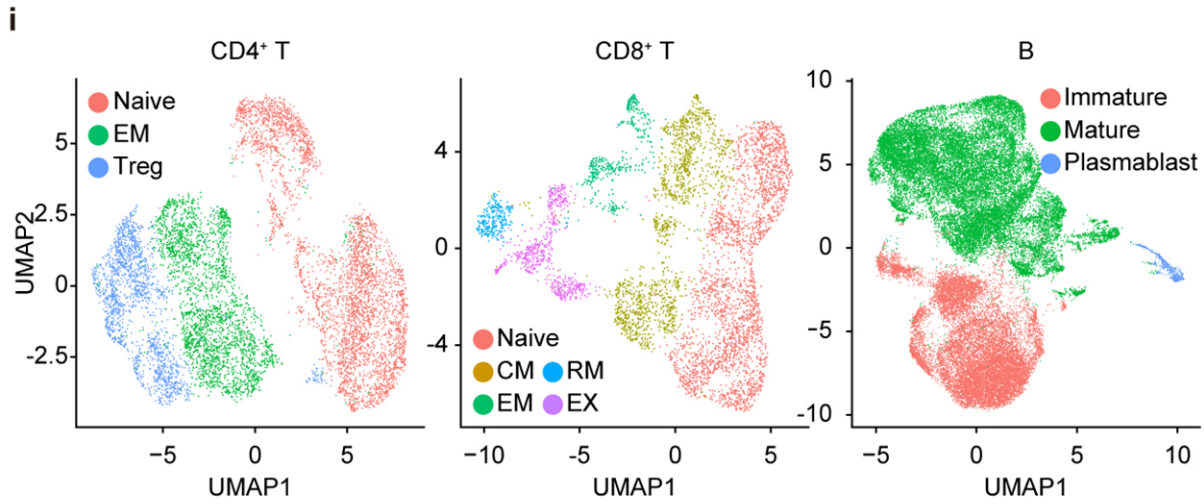


**i,** UMAP plot of subclustering of CD4⁺ T cells (left), CD8⁺ T cells (middle), and B cells (right).

**Supplementary Fig. 5j**

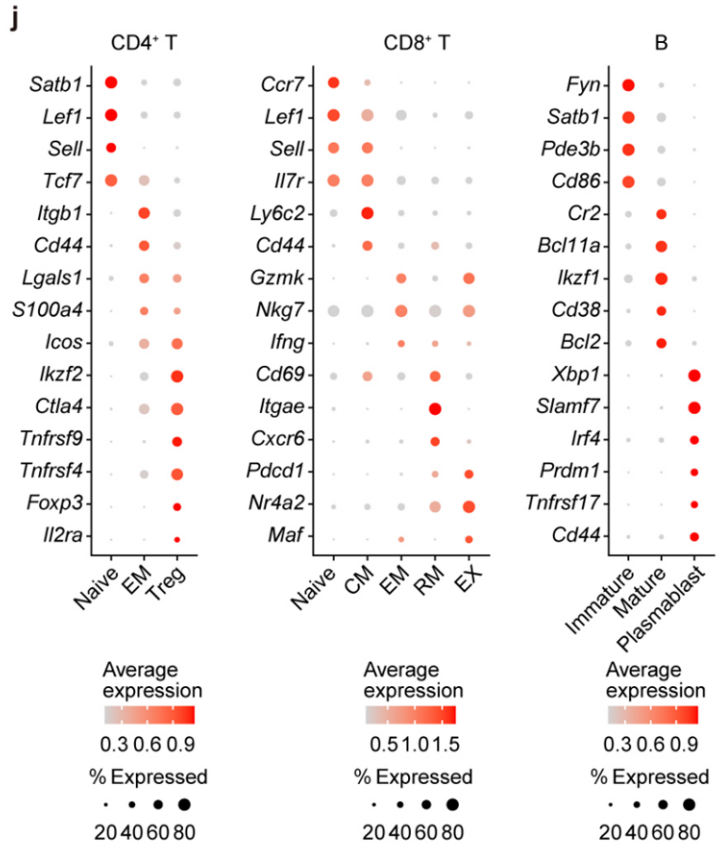


**j,** Bubble plot of representative mRNA markers for each CD4$^+$ T-cell (left), CD8$^+$ T-cell (middle), and B-cell (right) subcluster.

**Methods**

**(Page 37, line 759) Identification of cell clusters on scRNA-seq**

We applied the same normalization, dimensionality reduction and clustering pipeline as described above to each dataset of T/NK, B, and myeloid cells to identify subclusters within these broad cell types.

**#1-2**

This study used scRNA-seq to demonstrate the changes in myeloid cell types. The statistical analyses are needed to strengthen their findings. For ligand-receptor pairs and therapeutic targets highlighted, they should provide additional validation, such as flow cytometry analyses from their mouse models and clinical samples.

To address the reviewer's suggestion, we used a binomial test to evaluate the statistical significance of the $R_{o/e}$ analysis (ratio of observed cell number to expected

cell number) employed to investigate the distribution of myeloid cell subclusters in each group in scRNA-seq data. We also modified cut-off values used in the $R_{o/e}$ analysis as +++ indicates $R_{o/e} \geq 3$; ++, $2 \leq R_{o/e} < 3$; +, $1.5 \leq R_{o/e} < 2$; +/−, $0.67 \leq R_{o/e} < 1.5$; -, $0 \leq R_{o/e} < 0.67$. As a result, we confirmed that all clusters/subclusters with ++ and + showed a significantly increased proportion, whereas those with - showed a significantly decreased proportion in not only myeloid but also all other clusters/subclusters (**Fig. 4 and 5**).

We highlight CXCL16-CXCR6, CXCL9-CXCR3, and KLRG1 as important ligand-receptor pairs and/or therapeutic targets in this study. In the original manuscript, in addition to mouse scRNA-seq analysis, we have already showed increased CXCR6 and CXCR3 expressions using human bulk RNA-seq analysis (**new Fig. 5h**) as well as increased KLRG1 expression using flow cytometric analysis of mouse tumors (**Fig. 6b**) and human bulk RNA-seq analysis (**Fig. 6d**). As the reviewer suggested, we added flow cytometric analysis of CXCR6 and CXCR3 expressions in mouse tumors, which demonstrated increased expressions of these chemokine receptors in *Trp53*$^{-/-}$*LMP1*$^{+}$ tumor cells compared with *Trp53*$^{-/-}$ tumor cells (**Fig. 5g and Supplementary Fig. 6e**). We also performed immunohistochemical analysis of human samples and confirmed CXCR6, CXCR3, and KLRG1 expressions in human ENKTCL (**Fig. 5i, 6e, and Supplementary Fig. 7d**). Furthermore, we found that *LMP1* expression was positively correlated with *CXCL16* and *CXCL9* expressions in human RNA-seq data (**Supplementary Fig. 6g**). These results provide additional validation of CXCL16-CXCR6, CXCL9-CXCR3, and KLRG1 expression in mouse *Trp53*$^{-/-}$*LMP1*$^{+}$ tumors and human ENKTCL. Therefore, we have added the explanation and the data in **Results**, **Methods**, **Fig. 5g,i**, and **Supplementary Fig. 6e,g** in the revised manuscript as follows.

**Results**

**(Page 12, line 284)**

Flow cytometric analysis confirmed higher expressions of CXCR6 and CXCR3 in *Trp53*$^{-/-}$*LMP1*$^{+}$ tumor cells (**Fig. 5g and Supplementary Fig. 6e**). RNA-seq of human samples showed increased expressions of these chemokine ligands and receptors and their correlation with *LMP1* expression in ENKTCL (**Fig. 5h and Supplementary Fig. 6f,g**). We also validated the presence of CD11c$^{+}$ DC in the tumor microenvironment and CXCR6 and CXCR3 protein expressions in tumor cells by immunohistochemical analysis of human ENKTCL (**Fig. 5i and Supplementary Fig. 6h**).

**Fig. 5g**

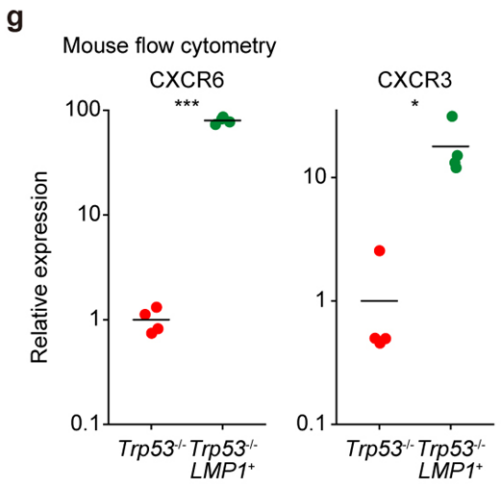


**g,** Relative CXCR6 (left) and CXCR3 (right) expressions in $Lin^{-}CD122^{+}$ cells from *Trp53*$^{-/-}$ (n = 4) and *Trp53*$^{-/-}$*LMP1*$^{+}$ (n = 4) tumors by flow cytometry.

**Fig. 5i**

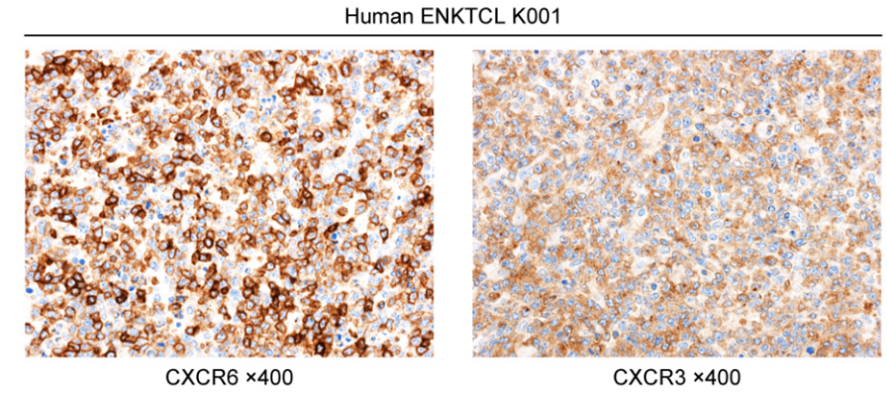


**i,** Representative images of CXCR6 (left) and CXCR3 (right) immunostaining in a human ENKTCL sample.

**Supplementary Fig. 6e**

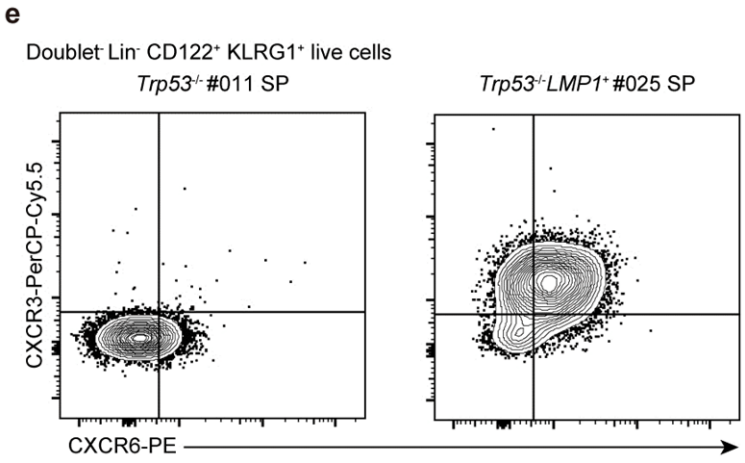


**e,** Representative plots of CXCR6 and CXCR3 expressions in Lin⁻CD122⁺ cells from *Trp53*$^{-/-}$ and *Trp53*$^{-/-}$*LMP1*$^{+}$ tumors.

**Supplementary Fig. 6g**

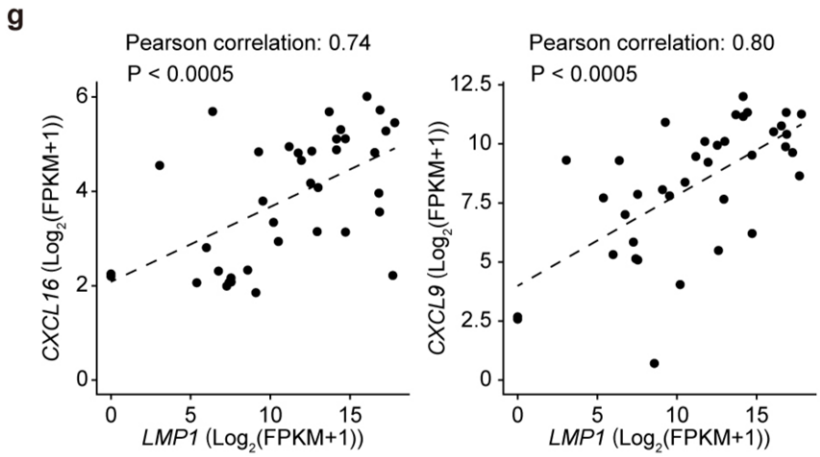


**g,** Correlation between *LMP1* expression and *CXCL16* (left) and *CXCL9* (right)gene expressions in 38 human ENKTCL samples. Pearson correlation test.

**Supplementary Table 9. Binominal test in each cell type in scRNA-seq analysis, related to Fig. 4, 5.**

**Methods**

**(Page 31, line 575) Histology**

Immunohistochemical analysis was performed using 3 μm-thick formalin-fixed paraffin embedded tissue sections from the tissue microarray. Slides were deparaffinized with xylene, followed by ethanol. After rehydration with water, antigen retrieval was

performed with Tris-EDTA buffer (pH 9.0) in a microwave oven at 95 °C for 20 min for KLRG1 and CD11c and for 40 min for CD49a, CXCR6, and CXCR3. After cooling and rinsing with buffer, slides were immunostained using Dako EnVision FLEX detection system (Agilent Technologies) on a Dako Autostainer Link48 (Agilent Technologies). Slides were incubated with antibodies as indicated in **Supplementary Table 18**. EBER in situ hybridization was performed using fluorescein isothiocyanate (FITC)-labeled EBV PNA Probe (Agilent Technologies) and anti-FITC antibody (Thermo Fisher Scientific).

**(Page 35, line 699) Bulk RNA-seq and analysis**

Expression for RefSeq genes and *LMP1* were calculated as fragments per kilobase of exon per million reads mapped values (FPKM). A detailed analysis of the human RNA-seq dataset was published elsewhere[32].

**(Page 38, line 770) Identification of cell clusters on scRNA-seq**

Statistical significance was assessed using the binomial test for each cell cluster.

**#1-3**

The authors observed elevated responses and outgoing signals in myeloid cells within tumors, suggesting a coordinated response in these cell types. Given the high abundance of these cells in the samples, further analyses are needed to determine whether specific subpopulations within these broader categories are the primary drivers of the cellular processes and communicating signals highlighted in this study.

We appreciate the reviewer's comment. As discussed in #1-1, we performed subclustering of myeloid cells again and identified 7 myeloid subclusters including Mono, MDSC, Macro, cDC1, cDC2, pDC, and mregDC. Using these new subclusters, we inferred cell-cell interactions using CellChat again and confirmed that IFN-II signaling was the most upregulated outgoing signaling in *Trp53*$^{-/-}$*LMP1*$^{+}$ tumor cells (**Fig. 5d**). In addition, we confirmed that CXC chemokine ligand (CXCL) signaling, particularly *Cxcl16-Cxcr6* and *Cxcl9-Cxcr3* signaling, was significantly upregulated in *Trp53*$^{-/-}$*LMP1*$^{+}$ tumor cells and mainly derived from myeloid cells (**Fig. 5d and Supplementary Fig. 6c**). Among myeloid subclusters, *Cxcl9-Cxcr3* signaling was derived from cDC1, while *Cxcl16-Cxcr6* signaling was derived from cDC1, Macro, and mregDC (**Fig. 5f**). Given that, among these myeloid subclusters, cDC1 was the only subcluster which was significantly increased in both the extranodal tissues (including the SG and other sites) and SP of *Trp53*$^{-/-}$*LMP1*$^{+}$ tumors (**Fig. 5b**), cDC1 is thought to be the main source of these chemokines. Therefore, we have revised the explanation

and the data in **Results**, **Fig. 5b,d,f**, and **Supplementary Fig. 6c** in the revised manuscript as follows.

**Results**

**(Page 12, line 283)**

This signaling included *Cxcl16-Cxcr6* and *Cxcl9-Cxcr3* signaling, which was mainly derived from myeloid cells, especially from cDC1 (**Fig. 5f**).

**Fig. 5b**

**b**

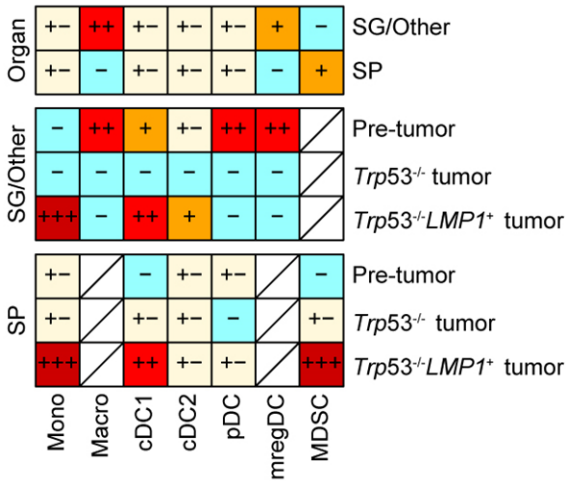


**b,** The distribution of myeloid subclusters in each group in the extranodal tissues and SP revealed by $R_{o/e}$ analysis. +++ indicates $R_{o/e} \geq 3$; ++, $2 \leq R_{o/e} < 3$; +, $1.5 \leq R_{o/e} < 2$; +/−, $0.67 \leq R_{o/e} < 1.5$; -, $0 \leq R_{o/e} < 0.67$.

**Fig. 5d**

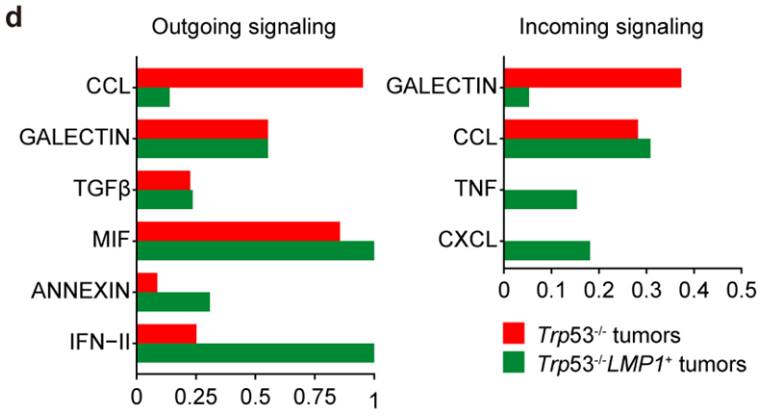


**d,** Comparison of outgoing and incoming signals between *Trp53*$^{-/-}$ and *Trp53*$^{-/-}$*LMP1*$^{+}$ tumors in CellChat analysis.

**Fig. 5f**

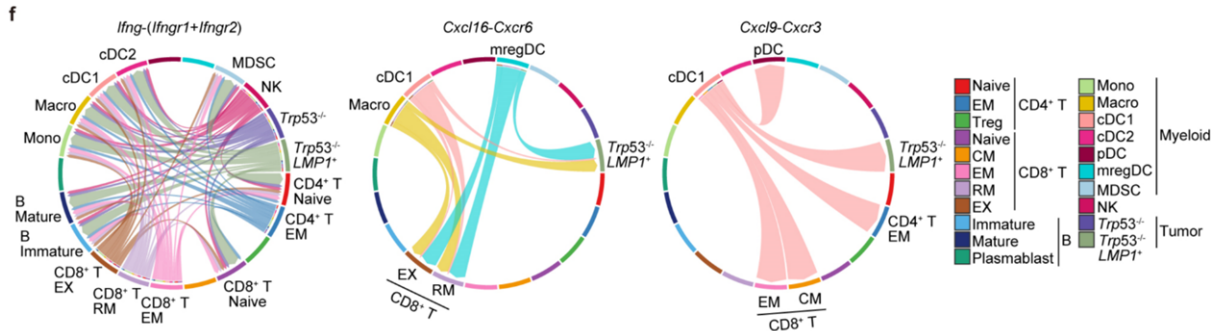


**f,** Chord diagram of *Ifng*-(*Ifngr1*+*Ifngr2*) (left)**,** *Cxcl16-Cxcr6* (middle), and *Cxcl9-Cxcr3* (right) signaling network across subclusters in *Trp53*$^{-/-}$ and *Trp53*$^{-/-}$*LMP1*$^{+}$ tumors.

**Supplementary Fig. 6c**

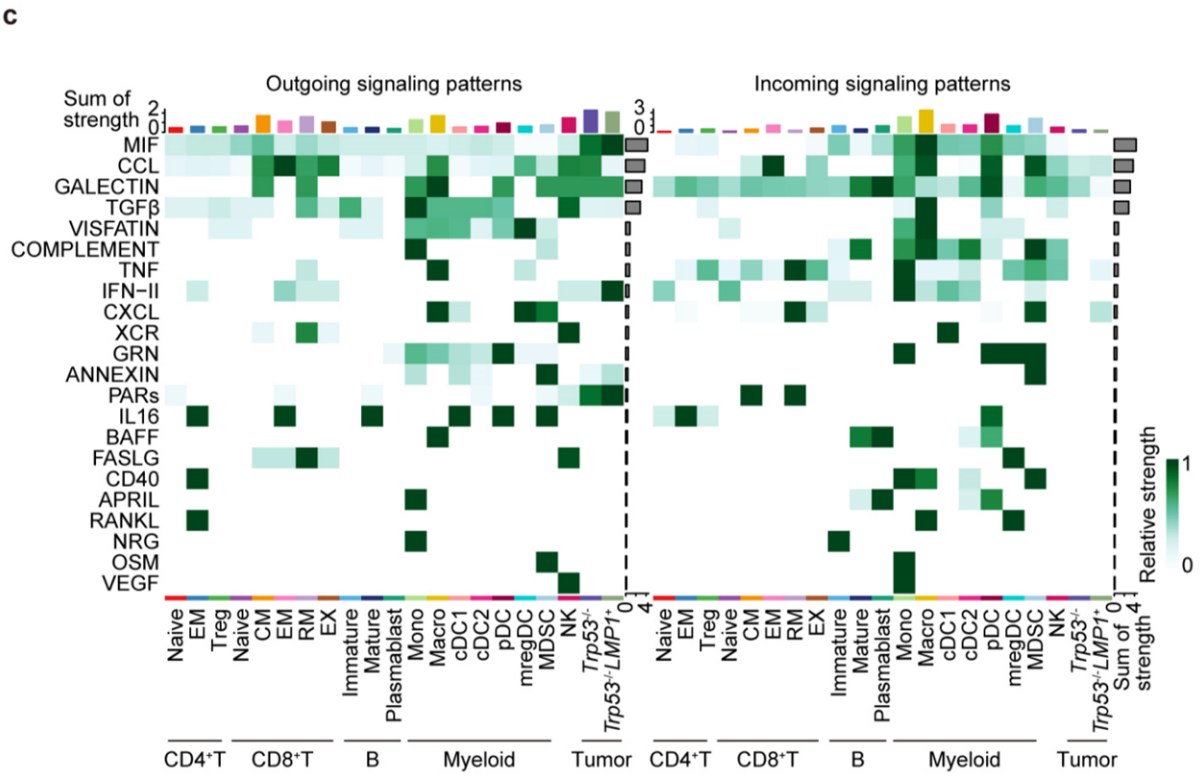


**c,** Heatmap showing relative strength of 16 pathways contributing to outgoing (left) or incoming (right) signaling of each cell cluster in CellChat analysis.

**#1-4**

The pro-tumor role of interactions between cDC and tumor cells via Cxcl16-Cxcr6 in this tumor model is not convincing. Specifically, there are comparable interactions between monocytes/macrophages and CD8 Tem cells. Additionally, Cxcr6 is critical for tumor control for CD8 cytotoxic T cells in previous studies (Pilato Cell, 2021). The authors simply described the signals in tumor cells but ignored those on CD8 T cells, which could also be the anti-tumor ones.

As the reviewer pointed out, besides *Trp53*$^{-/-}$*LMP1*$^{+}$ tumor cells, *Cxcl16-Cxcr6* signaling was transmitted to exhausted CD8$^{+}$ T (CD8$^{+}$ T EX) and resident memory CD8$^{+}$ T (CD8$^{+}$ T RM), while *Cxcl9-Cxcr3* signaling was transmitted to CD8$^{+}$ T EM, central memory CD8$^{+}$ T (CD8$^{+}$ T CM), CD4$^{+}$ T EM and pDC (**Fig. 5f**). As *Cxcl16-Cxcr6* and *Cxcl9-Cxcr3* signaling axis has been reported to promote anti-tumor responses of CD8$^{+}$ T cells in the tumor microenvironment[1,2], there is a possibility that these chemokine signaling pathways act through the interaction between myeloid cells and CD8$^{+}$ T cells. However, as i) the proportion of CD8$^{+}$ T cells was decreased in *Trp53*$^{-/-}$

*LMP1*$^{+}$ tumors (**Fig. 4c**) and ii) pharmacological inhibition of *Cxcl16-Cxcr6* signaling prolonged the survival of mice transplanted with *Trp53*$^{-/-}$*LMP1*$^{+}$ tumors (**new Fig. 5l**), it is more likely that these chemokine signaling pathways function through the interaction between myeloid cells and *Trp53*$^{-/-}$*LMP1*$^{+}$ tumor cells. To validate the latter observation, we assessed the effect of genetic inhibition of *Cxcl16-Cxcr6* signaling by transplanting *Trp53*$^{-/-}$*LMP1*$^{+}$ tumor cells into sub-lethally irradiated *Cxcl16* knockout mice and found that *Cxcl16* knockout also prolonged the survival (**Fig. 5m**). In addition, we treated *Trp53*$^{-/-}$*LMP1*$^{+}$ tumor cells with CXCL16 or CXCL9 in vitro and found that this treatment promoted the expansion of tumor cells (**Fig. 5j**). These observations confirm that *Cxcl16-Cxcr6* and *Cxcl9-Cxcr3* signaling can exert a direct effect on *Trp53*$^{-/-}$*LMP1*$^{+}$ tumor cells. Therefore, we have revised the explanation and the data in **Results**, **Methods**, and **Fig. 5j,m** in the revised manuscript as follows.

**Results**

**(Page 12, line 292)**

First, we examined the effect of CXCL16 or CXCL9 in vitro and found that these chemokines supported the expansion of *Trp53*$^{-/-}$*LMP1*$^{+}$ tumor cells (**Fig. 5j**).

**(Page 12, line 297)**

Similar findings were obtained when *Trp53*$^{-/-}$*LMP1*$^{+}$ tumor cells were transplanted into *Cxcl16* knockout mice (**Fig. 5m**).

**Fig. 5j**

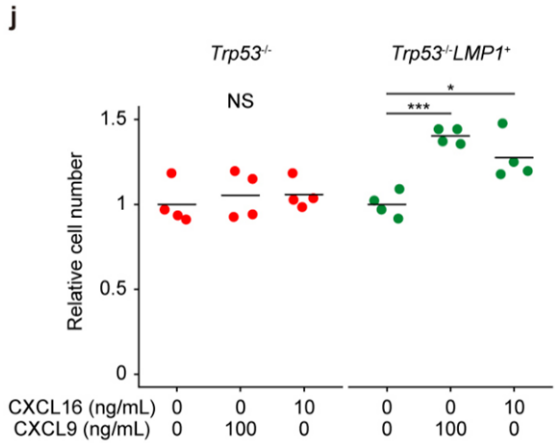


**j,** Relative cell number of *Trp53*$^{-/-}$ and *Trp53*$^{-/-}$*LMP1*$^{+}$ tumor cells 48 hours after CXCL16 or CXCL9 treatment at indicated concentrations (n = 4).

**Fig. 5m**

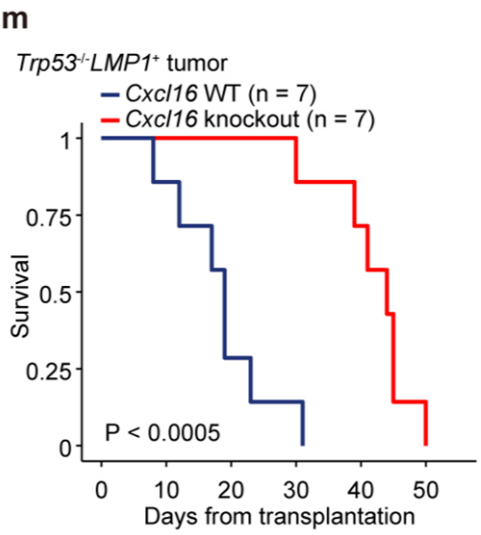


**m,** Kaplan-Meier survival curves of WT or *Cxcl16* knockout mice transplanted with $5\times10^5$ *Trp53*$^{-/-}$*LMP1*$^+$ tumor cells and administered with control vehicle or anti-KLRG1 antibody (n = 7 per group). Log-rank test.

**Methods**

**(Page 29, line 524) Mice**

C57BL/6-SR-PSOX (*Cxcl16* knockout) mice (nbio 196) were obtained from the Laboratory Animal Resource Bank of the National Institute of Biomedical Innovation, Health and Nutrition.

**(Page 32, line 600) In vitro chemokine Treatment**

To assess the effect of CXCL16 or CXCL9 on the proliferation of tumor cells, $1 \times 10^5$ Lin$^-$ *Trp53*$^{-/-}$ or Lin$^-$ *Trp53*$^{-/-}$*LMP1*$^+$ tumor cells were cultured in RPMI 1640 medium with 50% FBS, 1% PS, and 10 ng/mL IL-15 (PEPROTECH). The cells were treated with either no chemokine (control), 10 ng/mL CXCL16 (R&D Systems), or 100 ng/mL CXCL9 (R&D Systems). After 48 hours of culture, total cell count was determined using the automated cell counter Cell Counter model R1 (OLYMPUS) and normalized relative to the average of the control samples.

**#1-5**

In lines 112-115, the diagnostic foundation for a lethal hematopoietic neoplasm involving the SG should extend beyond reliance on complete blood count and macroscopic evaluation. A more robust diagnostic approach is essential to

conclusively assert that the hematopoietic neoplasm in NK-cell-specific Trp53 conditional knockout mice has manifested.

Furthermore, additional elucidation on the ENKTCL model within the GEMM is needed. A more comprehensive account of the developmental processes of ENKTCL in GEMM is necessary, accompanied by a detailed explanation of the methodologies employed to confirm the occurrence of ENKTCL in the mice. The authors should also compare the mutation signatures between mouse models and those from patients to validate their models further.

We appreciate the reviewer's comments. We agree that a robust diagnostic approach and its explanation is essential to confirm the occurrence of NK-cell tumors in the mice. Indeed, the diagnosis of ENKTCL is based on not only complete blood count (CBC) and macroscopic evaluation, but also histological examination, immunophenotyping with flow cytometry, secondary transplantation experiment, and integrative genetic analysis. Specifically, i) CBC showed mild leukocytosis, anemia, and thrombocytopenia (**Fig. 1b**); ii) Macroscopic evaluation demonstrated the enlargement of the SG, in addition to hepatosplenomegaly and occasional abdominal mass (**Fig. 1d**); iii) Histological examination revealed large-sized atypical lymphoid infiltration (**Fig. 1e**); iv) Flow cytometry identified a population of $Lin^{-}CD122^{+}NK1.1^{-}$ cells (**Fig. 1f**); v) Secondary transplantation showed that all recipients transplanted with tumors cells developed NK-cell tumors, resulting in early death (**new Fig. 1i**); and iv) Whole-exome sequencing (WES) identified many mutations and copy number alterations, confirming the clonality (**Supplementary Fig. 3c**). Taken together, NK-cell-specific *Trp53* disruption is considered to induce transplantable NK-cell lymphomas.

As the reviewer suggested, we have performed flow cytometric analysis of additional NK-cell transcription factors and markers. *Trp53*$^{-/-}$ tumor cells expressed NK-cell transcription factors (such as Eomes and T-bet) and lineage-committed NK-cell markers (such as CD43, CD146 [MCAM], CD226 [DNAM1], Ly6C, and CD62L) but lacked CD11b expression (**Fig. 1h and Supplementary Fig. 1d**), which supports the diagnosis of NK-cell tumors. Specifically, these cells are considered to resemble immature NK cells within the lineage-committed NK-cell compartment, although the differentiation process of tissue-resident NK cells has not been well characterized. We have also investigated mutation signatures using mouse NK-cell tumor and human ENKTCL WES data with the SigProfiler Bioinformatic Tools and the COSMIC v3.1 compendium. In total, we detected 464 mutations in 11 *Trp53*$^{-/-}$ and 14 *Trp53*$^{-/-}$*LMP1*$^{+}$ tumor samples by WES. These mutations mainly consisted of clock-like signatures (84.7%), but also contained signatures related to reactive oxygen species (15.3%)

(**Supplementary Fig. 4h**). Recently, we have performed comprehensive genetic analysis of 177 ENKTCL cases form France and Japan, in which WES was performed for 66 ENKTCL cases[3]. In total, we detected 3,386 mutations in 66 ENKTCL cases. These mutations mainly consisted of clock-like signatures (65.8%), but also contained signatures related to reactive oxygen species (18.1%). In addition, cosine similarity of mutations signatures between mouse NK-cell tumors and human ENKTCL was high (0.87) (**Supplementary Fig. 4h**). Therefore, it is plausible that mouse NK-cell tumors and human ENKTCL share similar mutational processes. These data strengthen the utility and relevance of our mouse models of NK-cell tumors. Therefore, we have revised the explanation and the data in **Results**, **Methods**, **Fig. 1h**, and **Supplementary Fig. 1d, 4h** in the revised manuscript as follows.

**Results**

**(Page 6, line 125)**

Flow cytometry of the tumors identified a population of Lin (Gr1, Ter119, CD19, and CD3)$^{-}$CD122$^{+}$NK1.1$^{-}$ cells, suggesting that these tumors were of NK-cell origin (**Fig. 1f**). The proportion of these cells was significantly increased in both the SG and SP in *Trp53*$^{-/-}$ tumor-bearing mice compared with age-matched WT controls (**Fig. 1g and Supplementary Fig. 1c**). These cells also expressed NK-cell transcription factors (such as Eomes and T-bet) and lineage-committed NK-cell markers (such as CD43, CD146 [MCAM], CD226 [DNAM1], Ly6C, and CD62L) but lacked CD11b expression (**Fig. 1h and Supplementary Fig. 1d**), resembling immature NK cells within the lineage-committed NK-cell compartment.

**(Page 10, line 220)**

We next characterized mutational processes in murine NK-cell tumors and revealed that clock-like (84.7%) and reactive oxygen species (15.3%) signatures were dominant, which is highly concordant with those found in human ENKTCL (**Supplementary Fig. 4h**).

## Fig. 1h

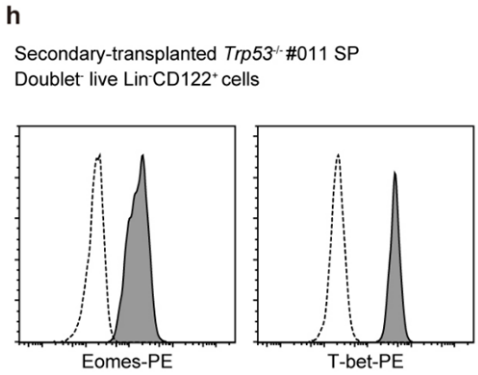


**h,** Representative histograms of Eomes and T-bet expression in *Trp53*$^{-/-}$ tumors in SP.

## Supplementary Fig. 1d

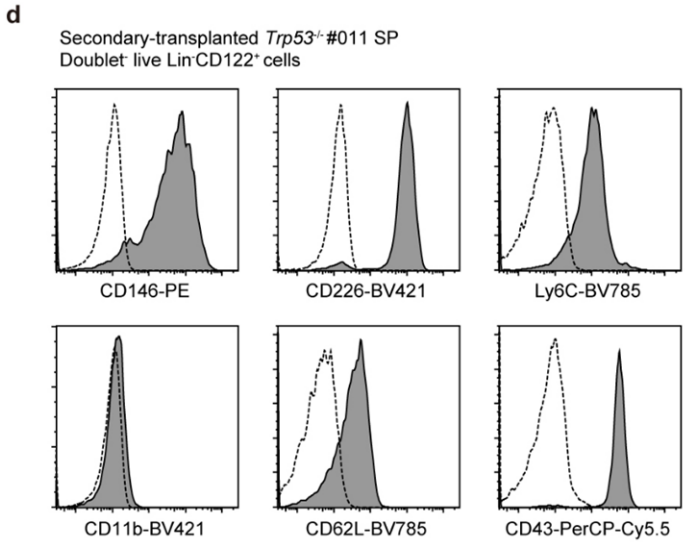


**d,** Representative histograms of CD146, CD226, LY6C, CD11b, CD62L and CD43 expression in in *Trp53*$^{-/-}$ tumors in SP.

**Supplementary Fig. 4h**

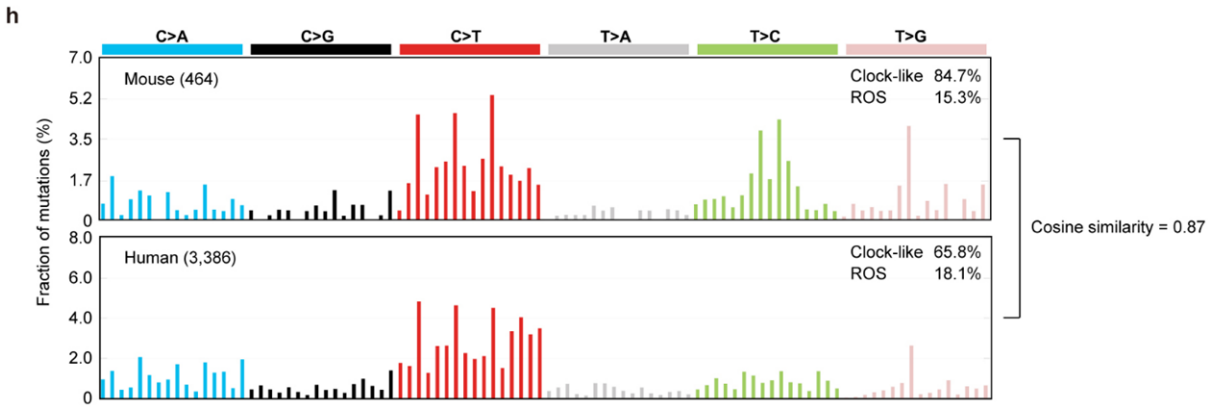


**h,** De novo mutational signatures extracted from 464 mutations in 25 mouse NK-cell tumors (11 *Trp53*$^{-/-}$ and 14 *Trp53*$^{-/-}$*LMP1*$^{+}$ tumors) and 3,386 mutations in 66 human ENKTCL samples[3] detected by WES. Known related etiologies are noted. Cosine similarities between mouse and human de novo signatures are shown.

## Methods

### (Page 30, line 567) Analysis of *Trp53*$^{-/-}$ and *Trp53*$^{-/-}$*LMP1*$^{+}$mice

The diagnosis of NK-cell tumors was based on CBC, macroscopic and histological examination, immunophenotyping with flow cytometry, evaluation of lymphomagenic potential in secondary transplantation, and whole-exome sequencing.

### (Page 31, line 592) Flow cytometry

For Intracellular flow cytometry of IFN-γ, Eomes, and T-bet expressions, we used the eBioscience™ Foxp3 / Transcription Factor Staining Buffer Set according to the manufacturer's instructions.

### (Page 34, line 662) Mutational signature

SigProfilerMatrixGenerator version 1.1.23 was used to categorize mutations into 96 classes and plot the mutational pattern, with the parameter "exome = True". We decomposed overall mutational pattern into 72 signatures from the COSMIC v3.1 compendium using SigProfilerExtractor version 1.1.0 with the default setting, and the proportion of clock-like (SBS1 and SBS5) and reactive oxygen species (SBS17a, SBS17b, and SBS18) signatures were calculated.

To compare the mutation pattern between mouse NK-cell tumors and human ENKTCL, we analyzed previously published WES data of 66 ENKTCL cases from our (accession number EGAS00001006906) and other studies (SRP057085 and

SRA2008200)[32]. Mutation calling and mutational signature analysis were performed in a similar manner to the mouse analysis.

**#1-6**

While the authors noted an upregulation of both Cxcl9-Cxcr3 and Cxcl16-Cxcr6 signaling in Trp53-/-LMP1+ tumor cells compared to Trp53-/- tumor cells, the manuscript predominantly delves into the investigation of Cxcl16-Cxcr6 signaling. The specific details or analyses pertaining to Cxcl9-Cxcr3 signaling are not as thoroughly explored in the provided information. The author should clarify their investigation of Cxcl9-Cxcr3 signaling, providing a detailed examination of its role and impact within the context of Trp53-/-LMP1+ tumor cells.

As the reviewer pointed out, we investigated the role of chemokine signaling by administering anti-CXCL16 antibody to mice transplanted with *Trp53*$^{-/-}$*LMP1*$^{+}$ tumor cells tumor cells. To address the reviewer's suggestion, we treated *Trp53*$^{-/-}$*LMP1*$^{+}$ tumor cells with CXCL16 or CXCL9 in vitro and found that this treatment promoted the expansion of tumor cells (**Fig. 5j**). In addition, we performed flow cytometric analysis of CXCR6 and CXCR3 expressions in mouse tumors, which demonstrated increased expressions of these chemokine receptors in *Trp53*$^{-/-}$*LMP1*$^{+}$ tumor cells compared with *Trp53*$^{-/-}$ tumor cells (**Fig. 5g and Supplementary Fig. 6e**). We also performed immunohistochemical analysis of human samples and confirmed CXCR6 and CXCR3 expressions in human ENKTCL (**Fig. 5i**). These observations confirm that not only *Cxcl16-Cxcr6* but also *Cxcl9-Cxcr3* signaling plays crucial roles in NK-cell lymphomagenesis. Therefore, we have revised the explanation and the data in **Results**, **Methods**, **Fig. 5g,i,j** and **Supplementary Fig. 6e** in the revised manuscript as follows.

**Results**

**(Page 12, line 284)**

Flow cytometric analysis confirmed higher expressions of CXCR6 and CXCR3 in *Trp53*$^{-/-}$*LMP1*$^{+}$ tumor cells (**Fig. 5g and Supplementary Fig. 6e**). RNA-seq of human samples showed increased expressions of these chemokine ligands and receptors and their correlation with *LMP1* expression in ENKTCL (**Fig. 5h and Supplementary Fig. 6f,g**). We also validated the presence of CD11c$^{+}$ DC in the tumor microenvironment and CXCR6 and CXCR3 protein expressions in tumor cells by immunohistochemical analysis of human ENKTCL (**Fig. 5i and Supplementary Fig. 6h**).

**(Page 12, line 292)**

First, we examined the effect of CXCL16 or CXCL9 in vitro and found that these chemokines supported the expansion of *Trp53*$^{-/-}$*LMP1*$^{+}$ tumor cells (**Fig. 5j**).

**Fig. 5g**

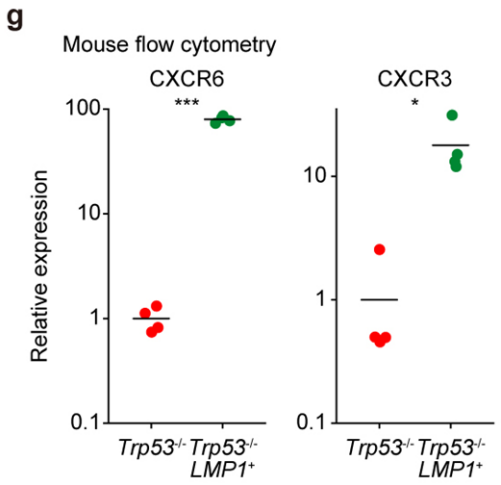


**g,** Relative CXCR6 (left) and CXCR3 (right) expressions in Lin$^{-}$CD122$^{+}$ cells from *Trp53*$^{-/-}$ (n = 4) and *Trp53*$^{-/-}$*LMP1*$^{+}$ (n = 4) tumors by flow cytometry.

**Fig. 5i**

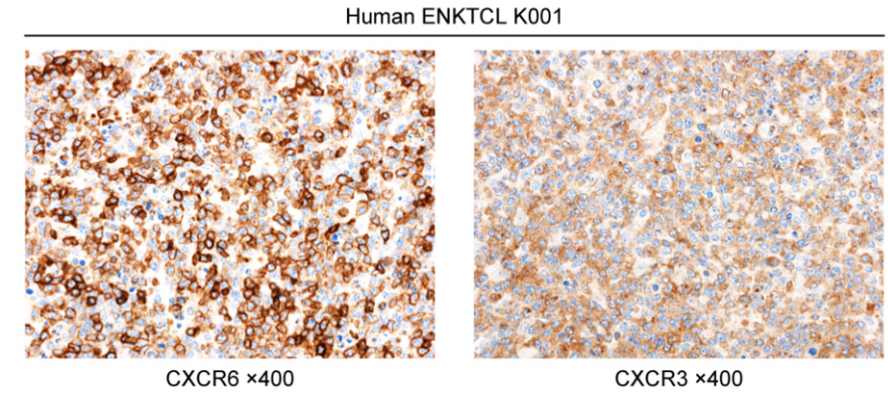


**i,** Representative images of CXCR6 (left) and CXCR3 (right) immunostaining in a human ENKTCL sample.

**Fig. 5j**

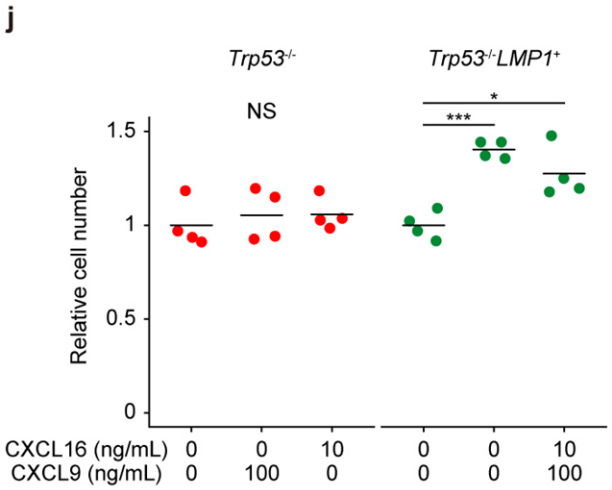


**j,** Relative cell number of *Trp53*$^{-/-}$ and *Trp53*$^{-/-}$*LMP1*$^{+}$ tumor cells 48 hours after CXCL16 or CXCL9 treatment at indicated concentrations (n = 4).

**Supplementary Fig. 6e**

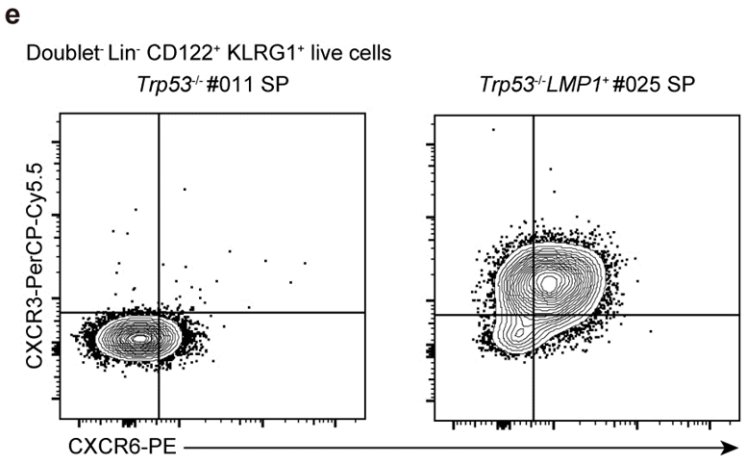


**e,** Representative plots of CXCR6 and CXCR3 expressions in Lin$^{-}$CD122$^{+}$ cells from *Trp53*$^{-/-}$ and *Trp53*$^{-/-}$*LMP1*$^{+}$ tumors.

**Methods**

**(Page 31, line 575) Histology**

Immunohistochemical analysis was performed using 3 µm-thick formalin-fixed paraffin embedded tissue sections from the tissue microarray. Slides were deparaffinized with xylene, followed by ethanol. After rehydration with water, antigen retrieval was performed with Tris-EDTA buffer (pH 9.0) in a microwave oven at 95 °C for 20 min for KLRG1 and CD11c and for 40 min for CD49a, CXCR6, and CXCR3. After cooling and rinsing with buffer, slides were immunostained using Dako EnVision FLEX

detection system (Agilent Technologies) on a Dako Autostainer Link48 (Agilent Technologies). Slides were incubated with antibodies as indicated in **Supplementary Table 18**.

**(Page 32, line 600) In vitro chemokine treatment**

To assess the effect of CXCL16 or CXCL9 on the proliferation of tumor cells, $1 \times 10^5$ Lin$^-$ *Trp53*$^{-/-}$ or Lin$^-$ *Trp53*$^{-/-}$*LMP1*$^+$ tumor cells were cultured in RPMI 1640 medium with 50% FBS, 1% PS, and 10 ng/mL IL-15 (PEPROTECH). The cells were treated with either no chemokine (control), 10 ng/mL CXCL16 (R&D Systems), or 100 ng/mL CXCL9 (R&D Systems). After 48 hours of culture, total cell count was determined using the automated cell counter Cell Counter model R1 (OLYMPUS) and normalized relative to the average of the control samples.

**#1-7**

In lines 275-281, the authors mentioned that Lin-KLRG1+ cells could develop into NK-cell tumors upon transplantation into secondary recipients, implying that KLRG1 expression can potentially identify tumor-initiating cells. However, there is a lack of discernible differences in the proportion of Lin-KLRG1+ cells between WT, Trp53-/-, and Trp53-/-LMP1+ during the pre-tumor stage.

The data presented suggests a plausible association between KLRG1 expression and tumor formation, but the conclusion that KLRG1 marks tumor-initiating cells requires additional substantiation. The authors should provide more evidence to support their claims regarding the role of KLRG1 in tumor initiation. This will strengthen the overall interpretation and validity of the findings related to KLRG1 expression in the context of tumorigenesis.

We appreciate the reviewer's comments. With respect to KLRG1 expression, we found that i) *Trp53*$^{-/-}$ and *Trp53*$^{-/-}$*LMP1*$^+$ tumor cells showed a marked increase of *Klrg1* expression in scRNA-seq data (**Fig. 6a**), ii) *Trp53*$^{-/-}$ and *Trp53*$^{-/-}$*LMP1*$^+$ tumors showed an increased proportion of Lin$^-$KLRG1$^+$ and Lin$^-$CD122$^+$KLRG1$^+$ cells by flow cytometry (**Fig. 6b and Supplementary Fig. 7b**), iii) only Lin$^-$KLRG1$^+$ cells developed into NK-cell tumors in secondary transplantation (**Fig. 6c**), iv) targeting tumor cells with anti-KLRG1 antibody was effective against *Trp53*$^{-/-}$ and *Trp53*$^{-/-}$*LMP1*$^+$ tumors (**new Fig. 6f,g**). These observations suggest that i) KLRG1 expression can effectively mark tumor cells and ii) KLRG1 is a promising therapeutic target against ENKTCL.

On the other hand, as the reviewer pointed out, there was almost no Lin$^-$KLRG1$^+$ and Lin$^-$CD122$^+$KLRG1$^+$ cells in SG and SP from WT, *Trp53*$^{-/-}$ and *Trp53*$^{-/-}$

*LMP1*$^{+}$ mice at the pre-tumor stage (**Fig. 6b and Supplementary Fig. 7b**). In addition, investigating the role of KLRG1 in NK-cell tumor initiation is out of scope of this paper and thus we did not claim that in the original manuscript. Therefore, we agree that the use of the term "tumor-initiating cells" may be misleading and thus have revised the sentences in **Results** and **Discussion** to remove the term "tumor-initiating cells" in the revised manuscript as follows.

**Results**

**(Page 13, line 317)**

Also we transplanted Lin-KLRG1- and Lin-KLRG1+ cells from Trp53-/- tumors into secondary recipients and found that only Lin-KLRG1+ cells developed into NK-cell tumors (Fig. 6c), suggesting that KLRG1 expression can mark tumor~~-initiating~~ cells.

**(Page 13, line 323)**

Then, we examined whether targeting tumor~~-initiating~~ cells with anti-KLRG1 antibody is effective against murine NK-cell tumors and found that anti-KLRG1 antibody treatment reduced the SP size to almost normal in mice transplanted with *Trp53*$^{-/-}$ tumors (**Supplementary Fig. 7d**).

**(Page 16, line 369)**

Here we have shown that KLRG1 is selectively expressed in mouse and human neoplastic cells ~~harboring tumor-initiating capacity~~ and anti-KLRG1 antibody can efficiently eliminate NK-cell tumors in mice.

**#1-8**

In Fig. 1e and Fig. 3c, histological examination for WT mice should be provided.

As the reviewer suggested, we performed histological examination of the SG and SP from WT mice and confirmed normal tissue architecture in these samples (**Supplementary Fig. 1b**). Therefore, we have added the data in **Supplementary Fig. 1b** in the revised manuscript as follows.

**Supplementary Fig. 1b**

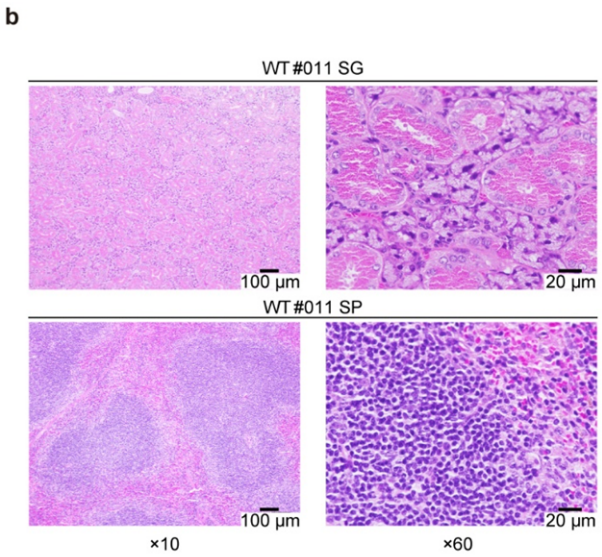


**b,** Representative image of hematoxylin and eosin staining of SG and SP from WT (at 8 weeks old) mice.

**#1-9**

In Fig. 1g, the proportion of Lin- cells between WT and Trp53-/- mice in SG did not show statistical significance. It seems to be a decreasing tendency in Trp53-/-. The author should explain the different alterations of such cells in SG and SP from the Trp53-/- models.

We apologize for the confusion regarding the proportion of $Lin^-$ cells in the SG. As the reviewer pointed out, the proportion of $Lin^-$ cells was comparable between WT and *Trp53*$^{-/-}$ mice. Indeed, $Lin^-$ cells contain not only NK cells but also various hematopoietic cell populations. Therefore, to avoid the confusion, we have removed the data regarding the proportion of $Lin^-$ cells in **Fig. 1g and Supplementary Fig. 4b** of the revise manuscript.

**#1-10**

In Fig. 3c, the authors should summarize the H&E staining data and perform statistical analysis.

In **Fig. 3c**, hematoxylin and eosin staining showed that *Trp53*$^{-/-}$*LMP1*$^{+}$ tumors showed myeloid infiltration and coagulative necrosis associated with vascular destruction. To

summarize the data, we counted the number of polymorphonuclear cells. As a result, we found that *Trp53*$^{-/-}$*LMP1*$^{+}$ tumors showed more extensive infiltration of polymorphonuclear cells than *Trp53*$^{-/-}$ tumors, as determined by a two-sided Welch's t-test (**Supplementary Fig. 4c**). Therefore, we have added the explanation and the data in **Methods**, and **Supplementary Fig. 4c** in the revised manuscript as follows.

**Results**

**(Page 9, line 212)**

Pathologically, *Trp53*$^{-/-}$*LMP1*$^{+}$ tumors showed more extensive myeloid infiltration and coagulative necrosis associated with vascular destruction, resembling the pathology of human ENKTCL (**Fig. 3c and Supplementary Fig. 4c**).

**Supplementary Fig. 4c**

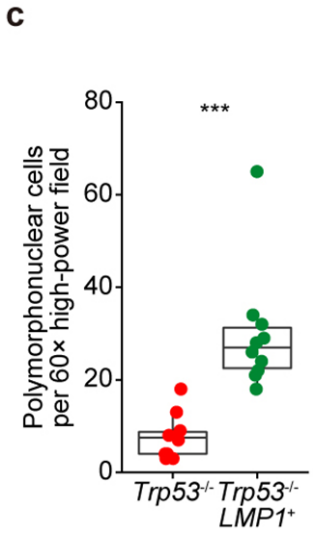


**c,** Number of polymorphonuclear cells per 60× high-power field in hematoxylin and eosin-stained sections of *Trp53*$^{-/-}$ and *Trp53*$^{-/-}$*LMP1*$^{+}$ tumors in SP. Five randomly chosen fields from each of two mice were examined per genotype.

**Methods**

**(Page 31, line 584) Histology**

To quantify myeloid cell infiltration, we counted polymorphonuclear cells in five 60× high-power field for each of two samples of *Trp53*$^{-/-}$ and *Trp53*$^{-/-}$*LMP1*$^{+}$ tumors.

**#1-11**

In Fig.4, more detailed analyses are needed to support their conclusion.

As described in detail in #1-1–4, we re-analyzed scRNA-seq data to support our conclusion. We thank for the reviewer's valuable comments.

**#1-12**

In Fig. 5, further experiments are needed to confirm that Trp53$^{-/-}$LMP1$^{+}$ tumors secrete more IFNγ, such as FACS or ELISA assay.

Using scRNA-seq data, we inferred cell-cell interactions using CellChat, which showed that IFN-II signaling (including only IFN-γ) was the most upregulated outgoing signaling in *Trp53*$^{-/-}$*LMP1*$^{+}$ tumor cells compared with *Trp53*$^{-/-}$ tumor cells (**Fig. 5d**). To address the reviewer's suggestion, we performed intracellular flow cytometry to assess IFN-γ expression at the protein level. We found that *Trp53*$^{-/-}$*LMP1*$^{+}$ tumor cells exhibit elevated IFN-γ protein expression compared with *Trp53*$^{-/-}$ tumor cells (**Fig. 5e**), confirming the scRNA-seq data. Therefore, we have added the explanation and the data in **Results**, **Methods**, and **Fig. 5e** in the revised manuscript as follows.

**Results**

**(Page 11, line 273)**

Intracellular flow cytometry confirmed elevated IFN-γ protein expression in *Trp53*$^{-/-}$ *LMP1*$^{+}$ tumor cells (**Fig. 5e**).

**Fig. 5e**

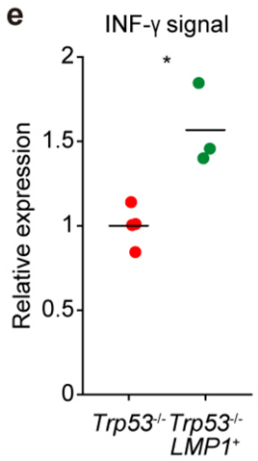


**e,** Relative IFN-γ expressions in Lin$^{-}$CD122$^{+}$ cells from *Trp53*$^{-/-}$ (n = 4) and *Trp53*$^{-/-}$ *LMP1*$^{+}$ (n = 3) tumors by intracellular flow cytometry.

**Methods**

**(Page 31, line 592) Flow cytometry**

For Intracellular flow cytometry of IFN-γ, Eomes, and T-bet expressions, we used the eBioscience™ Foxp3 / Transcription Factor Staining Buffer Set according to the manufacturer's instructions.

**Reviewer #2 (Remarks to the Author):**

Excellent manuscript outlining the role Trp53 and EBV-encoded latent membrane protein 1 expression NK-cell lymphomagenesis in mice and potential for KLRG1 targeting as a therapy. I think the manuscript is very solid as is. Congrats to the authors.

We appreciate the reviewer for the time and expertise in reviewing the manuscript and are very pleased that they consider that the manuscript is very solid as is.

**Reviewer #3 (Remarks to the Author):**

The manuscript by Koya et al. details a murine model of extranodal NK cell lymphoma, focused on the overexpression of TP53 in murine NK cells specifically. The authors demonstrated that knocking out Trp53 in all Ncr1 positive cells leads to expansion of NK cell tumors that are subsequently transplantable. When Lmp1 was overexpressed in the presence of Trp53 knockout, the tumors were more aggressive, yet maintained a similar pattern. Finally, use of a depleting antibody against the NK cell maturation marker, KLRG1, led to improved overall survival in the mice. Overall the studies were robust and provided extensive transcriptomic analysis of the murine model of Trp53 knockout, as well as additional ENKTCL human samples.

We appreciate the reviewer for the time and expertise in reviewing the manuscript and are very pleased that they consider "Overall the studies were robust and provided extensive transcriptomic analysis of the murine model of *Trp53* knockout, as well as additional ENKTCL human samples."

**#3-1**

First, human ENKTCL is defined by the presence of EBV within the NK cells, so the abundance of TP53 mutations in patients occurs in the backdrop of EBV-infection. How do the Trp53 KO cells compare to EBV-infected TP53 mutated NK cells in patients?

To address the reviewer's concern, we compared gene expression profiles between murine *Trp53*$^{-/-}$ NK-cell tumors and human *TP53*-mutated ENKTCL samples. In the original manuscript, gene set enrichment analysis (GSEA) of RNA-seq data showed upregulation of proliferation-related and MYC target gene signatures and downregulation of TNFα/NF-κB signaling and inflammatory signatures in *Trp53*$^{-/-}$ tumors (**Supplementary Fig. 3f**). Recently, we have performed comprehensive genetic analysis of 177 ENKTCL cases form France and Japan[3]. In this study, RNA-seq data were analyzed in 38 ENKTCL cases, among which 20 cases were also analyzed for genetic alterations. We performed GSEA analysis of the RNA-seq data comparing 18 *TP53* wild-type and 2 *TP53*-mutated ENKTCL samples and found upregulation of proliferation-related and MYC target gene signatures and downregulation of TNFα/NF-κB signaling and inflammatory signatures in *TP53*-mutated ENKTCL samples (**Supplementary Fig. 3g**). Therefore, the gene expression profiles of murine *Trp53*$^{-/-}$ NK-cell tumors closely mirror those of human *TP53*-mutated ENKTCL, suggesting that our mouse model faithfully recapitulates the molecular features of human ENKTCL. Therefore, we have added the explanation and the data in **Results**, **Methods**, and **Supplementary Fig. 3g** in the revised manuscript as follows.

**Results**

**(Page 9, line 193)**

RNA-seq showed the significant enrichment of proliferation-related and MYC target gene signatures in *Trp53*$^{-/-}$ tumors (**Supplementary Fig. 3f and Supplementary Table 5**), which is consistent with upregulated signatures in human *TP53*-mutated ENKTCL samples (**Supplementary Fig. 3g and Supplementary Table 6**).

**Supplementary Fig. 3g**

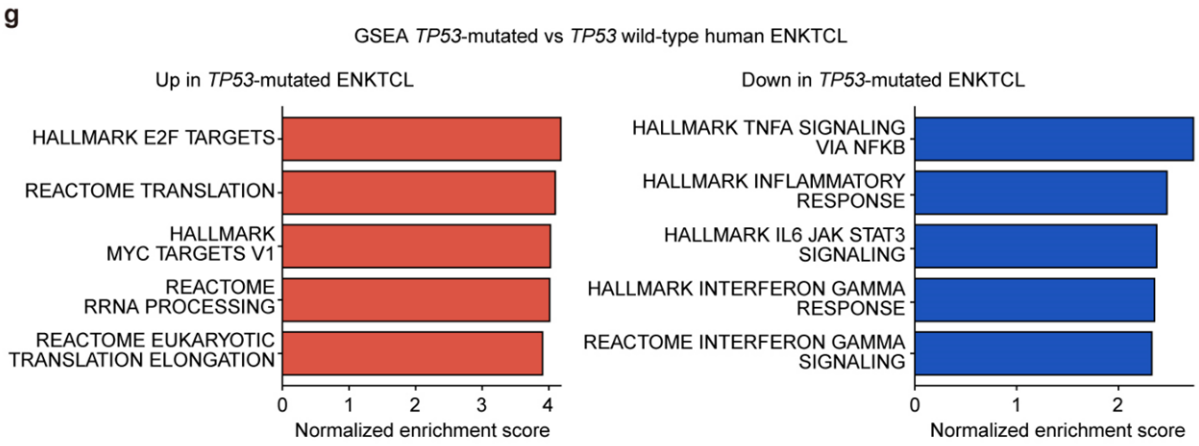


**g,** GSEA analysis of expression data comparing human *TP53* WT (n = 18) and *TP53*-mutated (n = 2) ENKTCL tumors.

**Supplementary Table 6. GSEA analysis of RNA-seq expression data comparing human *TP53* WT and *TP53*-mutated ENKTCL tumors, related to Supplementary Fig. 3.**

**#3-2**

Is the hypermethylation observed in EBV+ malignancies preserved in this model?

To address the reviewer's comment, we evaluated global DNA methylation status using MethylFlash Global DNA Methylation (5-mC) ELISA Easy Kit, but found no difference between normal NK cells, *Trp53*$^{-/-}$ tumor cells, and *Trp53*$^{-/-}$*LMP1*$^{+}$ tumor cells (**Reviewer-only Fig. 1**).

**Reviewer-only Fig. 1**

**[figure redacted]**

Global DNA methylation status of normal NK, *Trp53*$^{-/-}$ tumor, and *Trp53*$^{-/-}$*LMP1*$^{+}$ tumor cells (n = 4).

**#3-3**

The model of Trp53 KO with Lmp1 overexpression suggests there is more heterogeneity of KLRG1 expression as compared to the Trp53 KO alone-is there a difference in clonal expansion?

As the reviewer pointed out, the proportion of $Lin^-KLRG1^+$ and $Lin^-CD122^+KLRG1^+$ cells was slightly but not significantly lower in *Trp53*$^{-/-}$*LMP1*$^+$ tumors than in *Trp53*$^{-/-}$ tumors (**Fig. 6b and Supplementary Fig. 7b**), likely due to a higher proportion of samples with no or low tumor fraction (median allele frequency of < 10%) in *Trp53*$^{-/-}$*LMP1*$^+$ tumors (**new Supplementary Fig. 4d**). This is probably because *Trp53*$^{-/-}$*LMP1*$^+$ tumor cells can induce more prominent inflammatory responses, resulting in an earlier sacrifice of these mice. Therefore, we have added the explanation and the data in **Results** in the revised manuscript as follows.

**Results**
**(Page 13, line 310)**
Flow cytometric analysis confirmed an increased proportion of $Lin^-KLRG1^+$ and $Lin^-CD122^+KLRG1^+$ cells in *Trp53*$^{-/-}$ and *Trp53*$^{-/-}$*LMP1*$^+$ tumors, although the proportions were slightly lower in *Trp53*$^{-/-}$*LMP1*$^+$ tumors than in *Trp53*$^{-/-}$ tumors, probably due to more extensive inflammatory responses in *Trp53*$^{-/-}$*LMP1*$^+$ tumors (**Fig. 6b and Supplementary Fig. 7b**).

**#3-4**
Additional immunophenotyping of the model demonstrating protein expression of NK-associated TFs and maturation markers would further classify the stage of NK cells in the model.

As the reviewer suggested, we have performed flow cytometric analysis of additional NK-cell transcription factors and markers. *Trp53*$^{-/-}$ tumor cells expressed NK-cell transcription factors (such as Eomes and T-bet) and lineage-committed NK-cell markers (such as CD43, CD146 [MCAM], CD226 [DNAM1], Ly6C, and CD62L) but lacked CD11b expression (**Fig. 1h and Supplementary Fig. 1d**), which supports the diagnosis of NK-cell tumors. Specifically, these cells are considered to resemble immature NK cells within the lineage-committed NK-cell compartment, although the differentiation process of tissue-resident NK cells has not been well characterized. Therefore, we have revised the explanation and the data in **Results**, **Methods**, **Fig. 1h**, and **Supplementary Fig. 1d** in the revised manuscript as follows.

**Results**

**(Page 6, line 125)**

Flow cytometry of the tumors identified a population of Lin (Gr1, Ter119, CD19, and CD3)$^{-}$CD122$^{+}$NK1.1$^{-}$ cells, suggesting that these tumors were of NK-cell origin (**Fig. 1f**). The proportion of these cells was significantly increased in both the SG and SP in *Trp53*$^{-/-}$ tumor-bearing mice compared with age-matched WT controls (**Fig. 1g and Supplementary Fig. 1c**). These cells also expressed NK-cell transcription factors (such as Eomes and T-bet) and lineage-committed NK-cell markers (such as CD43, CD146 [MCAM], CD226 [DNAM1], Ly6C, and CD62L) but lacked CD11b expression (**Fig. 1h and Supplementary Fig. 1d**), resembling immature NK cells within the lineage-committed NK-cell compartment.

**Fig. 1h**

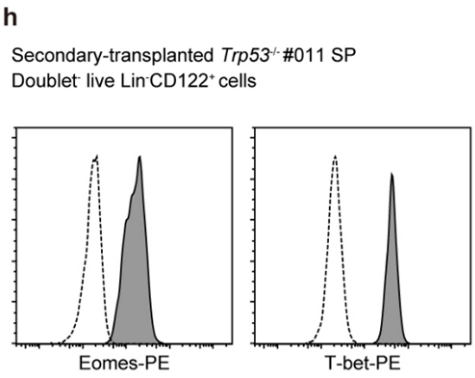


**h,** Representative histograms of Eomes and T-bet expression in *Trp53*$^{-/-}$ tumors in SP.

**Supplementary Fig. 1d**

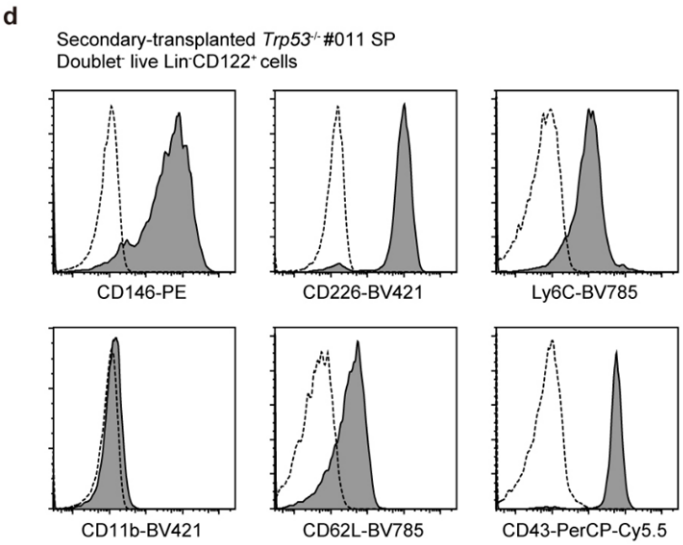

**d,** Representative histograms of CD146, CD226, LY6C, CD11b, CD62L and CD43 expression in in *Trp53*$^{-/-}$ tumors in SP.

**Methods**

**(Page 31, line 592) Flow cytometry**

For Intracellular flow cytometry of IFN-γ, Eomes, and T-bet expressions, we used the eBioscience™ Foxp3 / Transcription Factor Staining Buffer Set according to the manufacturer's instructions.

**#3-5**

For translational relevance, do human TP53 mutated ENKTL samples have elevated protein expression of KLRG1, and is this uniformly expressed like the mouse model or variable?

As the reviewer suggested, we examined KLRG1 expression in human ENKTCL by immunohistochemistry and confirmed its expression (**Fig. 6e and Supplementary Fig. 7d**). We observed high heterogeneity in KLRG1 protein expression among samples, with cases ranging from high positivity in almost all tumor cells to those with low positivity in a small fraction of cells. Therefore, we have added the explanation and the data in **Results**, **Methods**, **Fig. 6e, and Supplementary Fig. 7d** in the revised manuscript as follows.

**Results**

**(Page 13, line 319)**

We confirmed that *KLRG1* expression was upregulated in a substantial proportion of ENKTCL samples in human RNA-seq data (**Fig. 6d**), which was further supported by immunohistochemical analysis showing positive expression of KLRG1 in tumor cells in human ENKTCL, albeit with heterogeneity in KLRG1 positivity across samples. (**Fig. 6e and Supplementary Fig. 7d**).

**Discussion**

**(Page 16, line 369)**

Here we have shown that KLRG1 is selectively expressed in mouse and human neoplastic cells and anti-KLRG1 antibody can efficiently eliminate NK-cell tumors in mice.

**Fig. 6e**

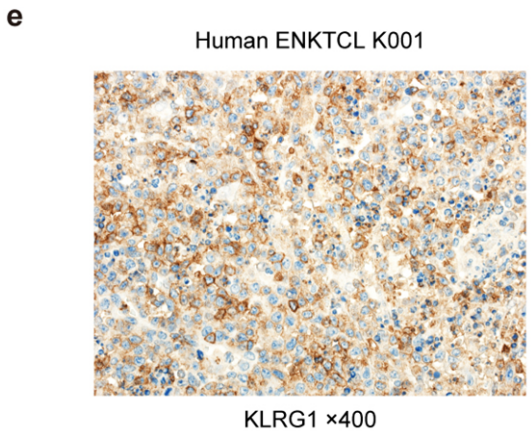


**e,** Representative image of KLRG1 immunostaining in a human ENKTCL sample.

**Supplementary Fig. 7d**

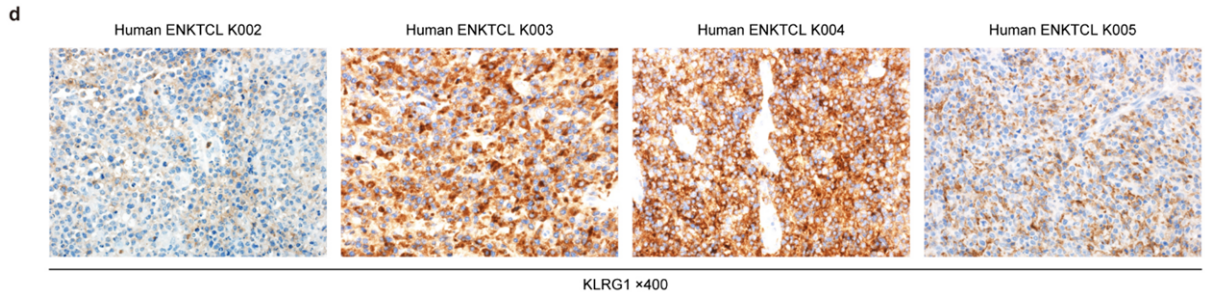


**d,** Representative images of KLRG1 immunostaining in four additional human ENKTCL samples.

**Methods**

**(Page 31, line 575) Histology**

Immunohistochemical analysis was performed using 3 µm-thick formalin-fixed paraffin embedded tissue sections from the tissue microarray. Slides were deparaffinized with xylene, followed by ethanol. After rehydration with water, antigen retrieval was performed with Tris-EDTA buffer (pH 9.0) in a microwave oven at 95 °C for 20 min for KLRG1 and CD11c and for 40 min for CD49a, CXCR6, and CXCR3. After cooling and rinsing with buffer, slides were immunostained using Dako EnVision FLEX detection system (Agilent Technologies) on a Dako Autostainer Link48 (Agilent Technologies). Slides were incubated with antibodies as indicated in **Supplementary Table 18**. EBER in situ hybridization was performed using fluorescein isothiocyanate (FITC)-labeled EBV PNA Probe (Agilent Technologies) and anti-FITC antibody (Thermo Fisher Scientific). To quantify myeloid cell infiltration, we

counted polymorphonuclear cells in five 60× high-power field for each of two samples of *Trp53*$^{-/-}$ and *Trp53*$^{-/-}$*LMP1*$^{+}$ tumors.

**#3-6**

Several prior studies have identified human tissue-resident NK cells as the cell of origin of extranodal NK lymphoma-comparing the findings in this murine model with recently published human data would be useful.

To address the reviewer's comment, we performed rigorous literature search, but found no study showing that tissue-resident NK cells are a cell-of-origin of ENKTCL. Therefore, we believe that our study is the first to demonstrate tissue-resident NK cells as a putative cell-of-origin of ENKTCL. We also examined the expression of a tissue-resident marker CD49a in human ENKTCL by immunohistochemistry and confirmed its expression (**Fig. 2g**). Therefore, we have added the explanation and the data in **Results**, **Methods**, and **Fig. 2g** in the revised manuscript as follows.

**Results**

**(Page 8, line 174)**

High expression of CD49a was detected in human ENKTCL by immunohistochemistry (**Fig. 2g and Supplementary Fig. 2k**).

**Fig. 2g**

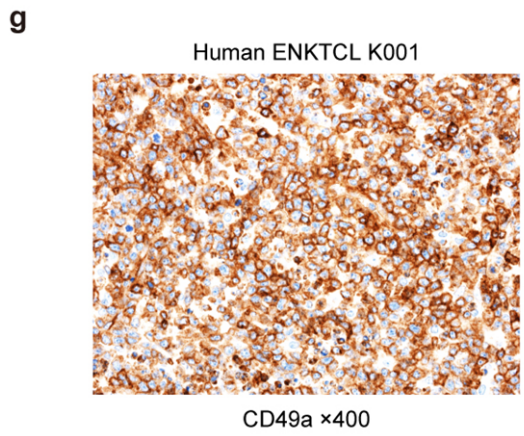


**g,** Representative image of CD49a immunostaining in a human ENKTCL sample.

**#3-7**

Support demonstrating relevance of myeloid infiltration with human NK lymphomas would support additional relevancy of the model.

As the reviewer suggested, we investigated the extent of myeloid infiltration using RNA-seq data of human ENKTCL samples. Specifically, we conducted a CIBERSORTx analysis on 38 human ENKTCL tumors and observed myeloid cell infiltration ranging from 1.2% to 65.4% in all tumors (**Supplementary Fig. 5g**). Furthermore, we found a positive correlation between *LMP1* expression of and the proportion of myeloid cells (**Supplementary Fig. 5h**). In addition, we performed immunohistochemical analysis of human ENKTCL (**Supplementary Fig. 6h**) samples and confirmed the infiltration of $CD11c^+$ DC into the tumor microenvironment. These observations provide additional relevance of our mouse models. Therefore, we have added the explanation and the data in **Results**, **Methods**, and **Supplementary Fig. 5g,h and 6h** in the revised manuscript as follows.

**Results**

**(Page 10, line 239)**

In addition, deconvolution of RNA-seq data of human ENKTCL revealed that myeloid cell infiltration was observed in all tumors and its extent was positively correlated with *LMP1* expression (**Supplementary Fig. 5g,h and Supplementary Table 10)**.

**(Page 12, line 288)**

We also validated the presence of $CD11c^+$ DC in the tumor microenvironment and CXCR6 and CXCR3 protein expressions in tumor cells by immunohistochemical analysis of human ENKTCL (**Fig. 5i and Supplementary Fig. 6h**).

## Supplementary Fig. 5g

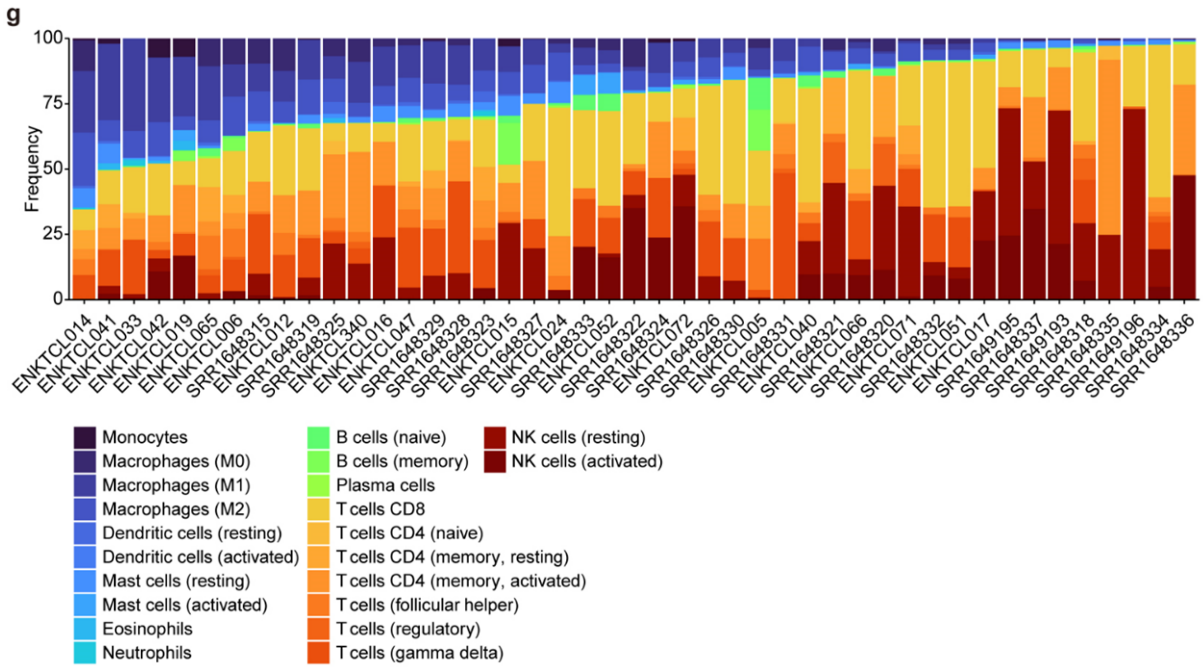


**g,** CIBERSORTx deconvolution of RNA-seq data of 38 human ENKTCL tumors.

## Supplementary Fig. 5h

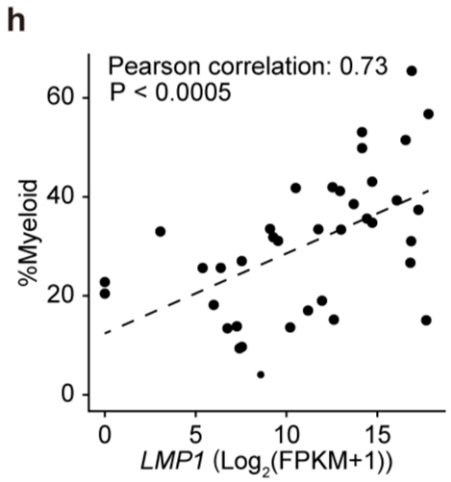


**h,** Correlation between *LMP1* expression and proportion of myeloid cells in 38 human ENKTCL tumors. Pearson correlation test.

**Supplementary Fig. 6h**

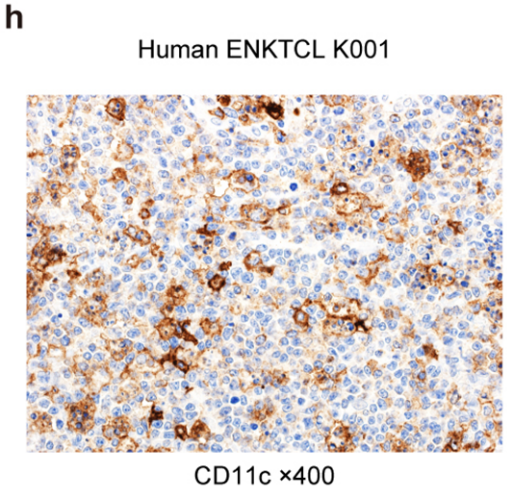


**h,** Representative image of CD11c immunostaining in a human ENKTCL sample.

**Methods**

**(Page 31, line 575) Histology**

Immunohistochemical analysis was performed using 3 µm-thick formalin-fixed paraffin embedded tissue sections from the tissue microarray. Slides were deparaffinized with xylene, followed by ethanol. After rehydration with water, antigen retrieval was performed with Tris-EDTA buffer (pH 9.0) in a microwave oven at 95 °C for 20 min for KLRG1 and CD11c and for 40 min for CD49a, CXCR6, and CXCR3. After cooling and rinsing with buffer, slides were immunostained using Dako EnVision FLEX detection system (Agilent Technologies) on a Dako Autostainer Link48 (Agilent Technologies). Slides were incubated with antibodies as indicated in **Supplementary Table 18**.

**(Page 36, line 715) Immune cell deconvolutoin using CIBERSORTx**

To estimate the proportions of different immune cell types, the FPKM values were uploaded to the CIBERSORTx online platform (https://cibersortx.stanford.edu/) for each cell type. The LM22 signature matrix was used with the following parameters; quantile normalization disabled, absolute run mode, and 100 permutations. The correlation between the proportion of myeloid cells and *LMP1* expression was assessed using Pearson's correlation test.

**#3-8**

The impact of KLRG1 depletion was modest in the model with Lmp1 overexpression-were there additional targets uncovered unique to this model which may correlate most closely with human NK lymphoma?

As the reviewer pointed out, the impact of anti-KLRG1 antibody on *Trp53*$^{-/-}$*LMP1*$^{+}$ tumors was modest (**new Fig. 6g**). Therefore, as the reviewer suggested, we explored another therapeutic target and identified further upregulation of MYC target gene signature in *Trp53*$^{-/-}$*LMP1*$^{+}$ tumors compared with *Trp53*$^{-/-}$ tumors (**Fig. 6h**), although this signature was significantly enriched even in *Trp53*$^{-/-}$ tumors compared with *Trp53*$^{-/-}$ Lin$^{-}$CD122$^{+}$ NK cells in SG (**Supplementary Fig. 3f**). In addition, 2 *Trp53*$^{-/-}$*LMP1*$^{+}$ tumors harbored focal amplifications involving *Myc* (**new Supplementary Fig. 4e**). MYC activation is frequently observed in human ENKTCL[4,5]. Therefore, we hypothesized that MYC inhibition is effective against NK-cell tumors and administered silvestrol, an eIF4A inhibitor known to inhibit Myc translation[6], in mice transplanted with *Trp53*$^{-/-}$*LMP1*$^{+}$ tumors. This treatment slightly but significantly prolonged the survival of tumor-bearing mice (**Fig. 6i**), highlighting the effectiveness of eIF4A inhibition in MYC-deregulated NK-cell lymphomas. Conspicuously, a combination of anti-KLRG1 antibody and silvestrol further extended the survival. These observations suggest that targeting KLRG1 alone and combined with MYC is a promising therapeutic approach against ENKTCL. Therefore, we have added the explanation and the data in **Abstract**, **Results**, **Methods**, **Discussion**, **Fig. 6h,i, and Supplementary Fig. 7f** in the revised manuscript as follows.

**Abstract**

**(Page 4, line 60)**

Extranodal NK/T-cell lymphoma (ENKTCL) is an Epstein-Barr virus (EBV)-related neoplasm preferentially involving the upper aerodigestive tract. Here we show that NK-cell-specific *Trp53* disruption in mice leads to the development of NK-cell lymphomas after long latency, which involve not only the hematopoietic system but also the salivary glands. Before tumor onset, *Trp53* knockout causes extensive gene expression changes, resulting in immature NK-cell expansion, exclusively in the salivary glands. Both human and murine NK-cell lymphomas express tissue-resident markers, suggesting tissue-resident NK cells as their cell-of-origin. Murine NK-cell lymphomas show recurrent *Myc* amplifications and upregulation of MYC target gene signatures. EBV-encoded latent membrane protein 1 expression accelerates NK-cell lymphomagenesis and causes diverse microenvironmental changes, particularly myeloid propagation, through interferon-γ signaling. In turn, myeloid cells support

tumor cells via CXCL16-CXCR6 signaling and its inhibition is effective against NK-cell tumors in vivo. Remarkably, KLRG1-expressing cells expand in the tumor and are capable of repopulating tumors in secondary recipients. Furthermore, targeting KLRG1 alone or combined with MYC inhibition using an eIF4 inhibitor is effective against NK-cell tumors. Therefore, our observations provide insights into the pathogenesis and highlight novel therapeutic targets, including CXCL16, KLRG1, and MYC, in ENKTCL, which can help improve its diagnostic and therapeutic strategies.

**Results**

**(Page 14, line 330)**

As the effectiveness of anti-KLRG1 antibody was modest against *Trp53*$^{-/-}$*LMP1*$^{+}$ tumors, we further explored another therapeutic target and identified further upregulation of MYC target gene signature in *Trp53*$^{-/-}$*LMP1*$^{+}$ tumors compared with *Trp53*$^{-/-}$ tumors in scRNA-seq data (**Fig. 6h, Supplementary Fig. 7f and Supplementary Table 15**), although the MYC target gene signature was enriched even in *Trp53*$^{-/-}$ tumors. Therefore, we administered silvestrol, an eIF4A inhibitor known to inhibit Myc translation[17], in mice transplanted with *Trp53*$^{-/-}$*LMP1*$^{+}$ tumors. This treatment slightly prolonged the survival of tumor-bearing mice (**Fig. 6i**). Conspicuously, a combination of anti-KLRG1 antibody and silvestrol further extended the survival (**Fig. 6i**). These observations suggest that targeting KLRG1 alone and combined with MYC is a promising therapeutic approach against ENKTCL.

**Discussion**

**(Page 16, line 376)**

Another important therapeutic target identified in this study is MYC. We have demonstrated that *Myc* is genomically and/or transcriptionally activated in *Trp53*$^{-/-}$ tumors and further deregulated in *Trp53*$^{-/-}$*LMP1*$^{+}$ tumors. Moreover, MYC inhibition with an eIF4A inhibitor strongly enhanced the efficacy of anti-KLRG1 antibody even in *Trp53*$^{-/-}$*LMP1*$^{+}$ tumors. As MYC activation is common in human ENKTCL[9,15], combined targeting of KLRG1 and MYC can be a promising therapeutic strategy against ENKTCL.

In conclusion, using GEMM recapitulating the human disease, we have delineated the cell-of-origin and microenvironmental changes and exploited novel therapeutic targets, including CXCL16, KLRG1, and MYC, for ENKTCL. These observations prove that our mouse models will serve as valuable tools for elucidating the pathogenic mechanisms and refining diagnostic and therapeutic strategies in ENKTCL.

## Fig. 6h

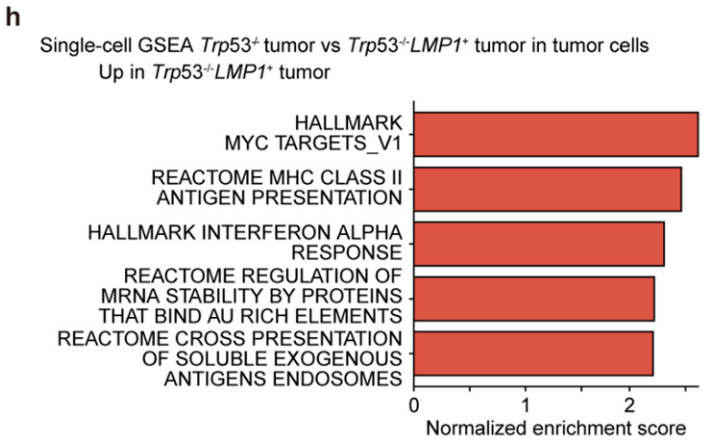


**h,** GSEA analysis of scRNA-seq data comparing *Trp53*$^{-/-}$ and *Trp53*$^{-/-}$*LMP1*$^{+}$ malignant NK cells. Top five upregulated signatures in *Trp53*$^{-/-}$*LMP1*$^{+}$ malignant NK cells are shown. Signatures with FDR < 0.25 are considered significant.

## Fig. 6i

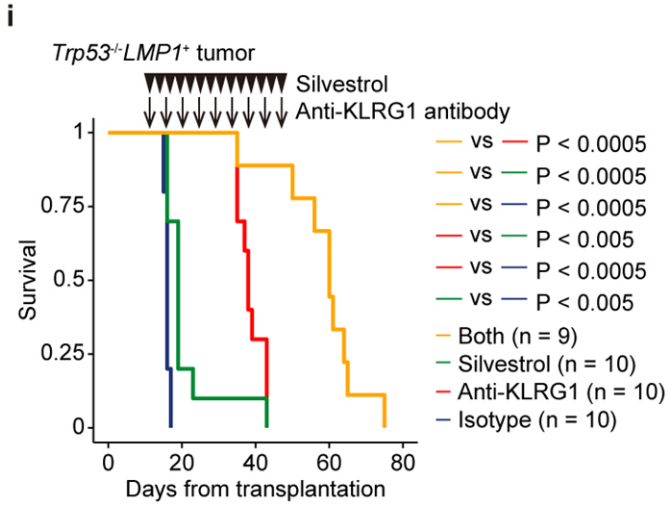


**i,** Kaplan-Meier survival curves of mice transplanted with $5\times10^5$ *Trp53*$^{-/-}$*LMP1*$^{+}$ tumor cells and administered with control vehicle, silvestrol, anti-KLRG1 antibody, or both (n = 10 for control, silvestrol, and anti-KLRG1 antibody; n = 9 for both). Log-rank test.

## Supplementary Fig. 7f

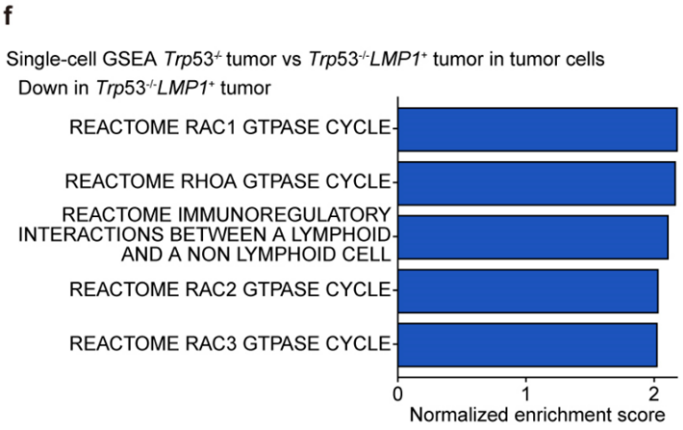


**f,** GSEA analysis of scRNA-seq data comparing *Trp53*$^{-/-}$ and *Trp53*$^{-/-}$*LMP1*$^{+}$ malignant NK cells. Top five downregulated signatures in *Trp53*$^{-/-}$*LMP1*$^{+}$ malignant NK cells are shown.

**Supplementary Table 15. GSEA analysis of scRNA-seq expression data comparing *Trp53*$^{-/-}$ and *Trp53*$^{-/-}$*LMP1*$^{+}$ malignant NK cells, related to Fig. 6 and Supplementary Fig. 7.**

### Methods

**(Page 33, line 627) Tumor models and in vivo treatment**

Silvestrol (MCH MedChemexpress, HY-13251) was dissolved in 5% dimethyl sulfoxide and stocked. Each stock was suspended in 5.2% PEG400, 5.2% Tween 80, and 84.6% dd$H_2O$ and 0.25 mg/kg of silvestrol was administered intraperitoneally every other day beginning from day 7 to day 37 post-transplantation.

## References


1 Di Pilato, M. *et al.* CXCR6 positions cytotoxic T cells to receive critical survival signals in the tumor microenvironment. *Cell* **184**, 4512-4530.e4522 (2021). https://doi.org/10.1016/j.cell.2021.07.015

2 Chow, M. T. *et al.* Intratumoral Activity of the CXCR3 Chemokine System Is Required for the Efficacy of Anti-PD-1 Therapy. *Immunity* **50**, 1498-1512.e1495 (2019). https://doi.org/10.1016/j.immuni.2019.04.010

3 Ito, Y. *et al.* Comprehensive genetic profiling reveals frequent alterations of driver genes on the X chromosome in extranodal NK/T-cell lymphoma. *Cancer Res* (2024). https://doi.org/10.1158/0008-5472.Can-24-0132

4 Xiong, J. *et al.* Genomic and Transcriptomic Characterization of Natural Killer T Cell Lymphoma. *Cancer Cell* **37**, 403-419.e406 (2020). https://doi.org/10.1016/j.ccell.2020.02.005

5 Oishi, N. *et al.* Genetic and immunohistochemical profiling of NK/T-cell lymphomas reveals prognostically relevant BCOR-MYC association. *Blood Adv* **7**, 178-189 (2023). https://doi.org/10.1182/bloodadvances.2022007541

6 Cerezo, M. *et al.* Translational control of tumor immune escape via the eIF4F-STAT1-PD-L1 axis in melanoma. *Nat Med* **24**, 1877-1886 (2018). https://doi.org/10.1038/s41591-018-0217-1

**Response to Reviewer Comments**

**NCOMMS-24-12212-T**
**Modeling NK-cell lymphoma in mice reveals its cell-of-origin, microenvironmental changes, and therapeutic targets.**

We thank the reviewers for their insightful comments and suggestions, which have helped to significantly improve our manuscript again. We believe that our new data and discussion address all of the reviewer's suggestions. Each of the reviewers' specific comments are addressed in full below.

**Reviewer #1 (Remarks to the Author):**
The authors have provided detailed explanations and performed additional experiments, effectively addressing my previous concerns.

We appreciate the reviewer for the time and expertise in reviewing the manuscript and are very pleased that he/she considers that our detailed explanations and additional experiments effectively address his/her previous concerns.

**#1-1**
Regarding the analyses, the manuscript has been improved to achieve a higher resolution in identifying cell populations. However, the selection of markers for several populations presented in the figures remains suboptimal, compromising the reliability of their annotations. For instance, Cd209a and Cd300a would be more appropriate markers for cDC2, Ifng and Tbx21 for CD4 Th1 cells, and Havcr2, Lag3, Entpd1, and Tox for Tex cells. The authors should conduct a thorough investigation to identify and utilize more appropriate markers for these cell populations.

We sincerely appreciate the reviewer's insightful suggestions. As per your recommendations, we have added the following mRNA markers:

For cDC2: *Cd209a* and *Cd300a*
For $CD4^+$ T EM cells: *Ifng* and *Tbx21*
For $CD8^+$T EX cells: *Havcr2*, *Lag3*, *Entpd1*, and *Tox*

In addition, we have performed an additional comprehensive literature review to identify and utilize more appropriate mRNA markers for various subclusters and incorporated the following mRNA markers:

For $CD4^+$T Naive: *Foxp1* (Wang et al. 2014)[1]
For $CD8^+$T EM: *Cx3cr1* (Böttcher et al. 2015)[2]

For CD8$^+$T RM: *Cdh1* (Hayward et al. 2020)[3]

For Macrophages: *Mafb* (Vanneste et al. 2023)[4]

For cDC1: *Tlr3* (Luber et al. 2010)[5]

We are pleased to report that these additional markers (highlighted in red) are differentially expressed in their relevant subclusters, as shown in **Supplementary Fig. 5j and 6a**. We believe that these changes significantly enhance the reliability of the cell cluster/subcluster annotations. Therefore, we have added the data in **Supplementary Fig. 5j and 6a** in the revised manuscript as follows.

**Supplementary Fig. 5j**

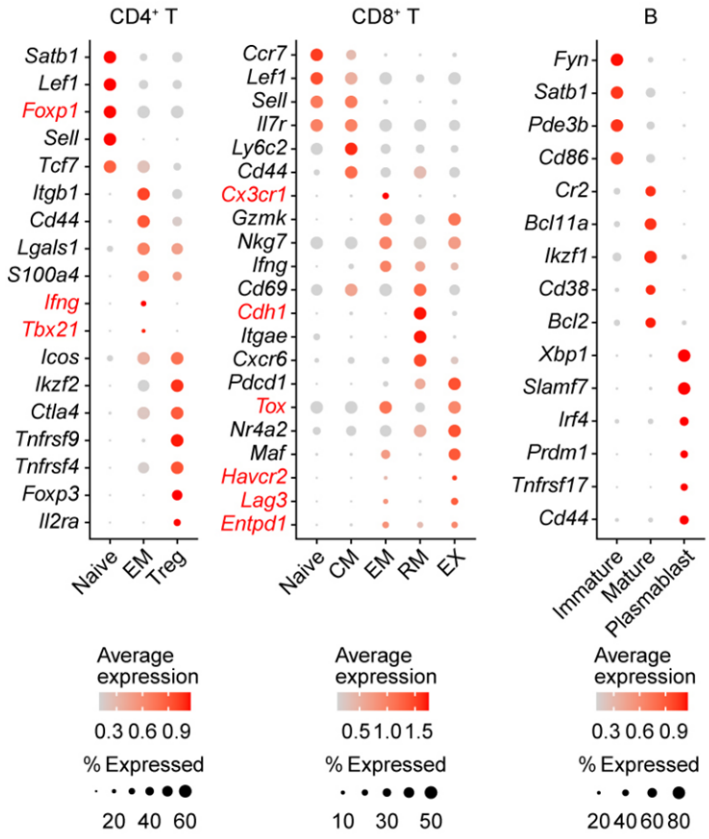


**j,** Bubble plot of representative mRNA markers for each CD4$^+$ T-cell (left), CD8$^+$ T-cell (middle), and B-cell (right) subcluster.

**Supplementary Fig. 6a**

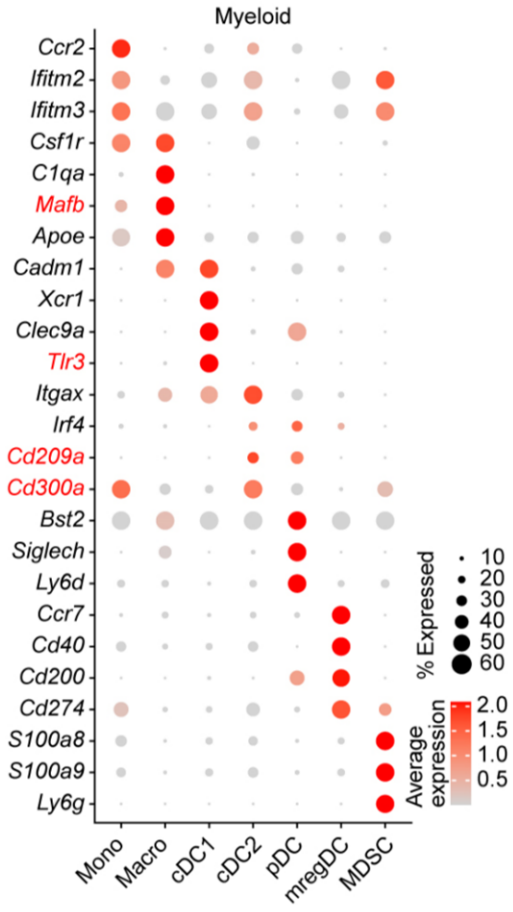


**a,** Bubble plot of representative mRNA markers for each myeloid cell subcluster.

**#1-2**

Additionally, the use of binomial-based tests for enrichment analysis is not optimal for robust comparisons between groups. Given that changes in cell abundance are a key finding of this study, it is imperative to include biological replicates and apply t-tests or Wilcoxon tests to strengthen the evidence supporting these changes.

We appreciate the reviewer's insightful comment. We acknowledge that t-test or Wilcoxon test would be more robust for comparing the proportion between groups. Due to the limited number of samples in each group, these statistical tests are not feasible in our single-cell analysis (**Fig. 4c and 5b**). In addition, we regret that increasing the number of samples for single-cell analysis is not possible at this stage of revision.

However, there have been several mouse single-cell studies in high-impact journals that deal with similar sample size constraints by performing Ro/e analysis without additional statistical tests. For example: (i) Xue et al. (Nature. 2022) performed

scRNA-seq analysis on peripheral blood, tumor-adjacent liver, and tumor samples from six mice. They identified 12 neutrophil clusters and demonstrated clear tissue specificity among these clusters using only Ro/e analysis without performing statistical tests[6]. (ii) Liu et al. (Nat Commun. 2022) conducted scRNA-seq analysis on tumor samples from WT and *Batf3*$^{-/-}$ mice (leading to cDC1 deficiency) with or without CD39 inhibitor treatment (three mice per group). They showed significant changes in cDC1 and migratory DC proportions across different conditions using only Ro/e analysis without performing statistical tests[7]. Given these recent practices in high-impact publications, we believe that our presentation of the distribution of cell clusters/subclusters in single-cell analyses is an acceptable approach and provides valuable information despite the limited sample number.

In addition, to address the limitation of sample size in our single-cell analyses, we have already conducted flow cytometry analyses with more samples (= biological replicates) from SG and SP of WT, *Trp53*$^{-/-}$, and *Trp53*$^{-/-}$*LMP1*$^{+}$ mice at the pre-tumor stage (at 8 weeks old), *Trp53*$^{-/-}$ tumors in SG and SP, and *Trp53*$^{-/-}$*LMP1*$^{+}$ tumors in SG and SP, allowing us for more robust statistical comparisons, in initial submission. Specifically, we obtained statistically significant findings using two-sided Welch's t-test as follows (**Fig. 4d**): (i) *Trp53*$^{-/-}$ and/or *Trp53*$^{-/-}$*LMP1*$^{+}$ tumors showed a lower proportion of CD4$^{+}$ and CD8$^{+}$ T cells in SG and/or SP compared to the pre-tumor stage; (ii) *Trp53*$^{-/-}$*LMP1*$^{+}$ tumors showed a marked increase of myeloid cells in SG and SP compared to the pre-tumor stage and even *Trp53*$^{-/-}$ tumors. These observations complement and validate the key findings of our single-cell analyses in a statistically sound manner.

To further validate the key findings of this study, we performed additional flow cytometry analysis for cDC1 in this revision (**Supplementary Fig. 6b**), because cDC1 is a cell type of particular interest in our study as (i) cDC1 shows a marked increase in both SG and SP from *Trp53*$^{-/-}$*LMP1*$^{+}$ tumors compared to the pre-tumor stage and even *Trp53*$^{-/-}$ tumors. (**Fig. 5b**); (ii) cDC1 is one of the main receivers of IFN-II signaling in the tumor microenvironment (**Fig. 5f**); and (iii) cDC1 is a major source of CXCL signaling, which is significantly upregulated in *Trp53*$^{-/-}$*LMP1*$^{+}$ tumors (**Fig. 5d,f**). Through this analysis, we confirmed the marked increase of cDC1 in *Trp53*$^{-/-}$*LMP1*$^{+}$ tumors by two-sided Welch's t-test.

Thus, we believe that these flow cytometric analyses, including additional one regarding cDC1, provide statistical validation and strengthen the evidence to support the substantial changes of important cell types, particularly myeloid cell expansion, in the tumor microenvironment in our NK-cell tumor mouse models. Therefore, we have added the explanation and the data in in **Results and Supplementary Fig. 6b** in the revised manuscript as follows.

**Results**

**(Page 11, line 262)**

The increase of cDC1 was confirmed by flow cytometric analysis (**Supplementary Fig. 6b**).

**Supplementary Fig. 6b**

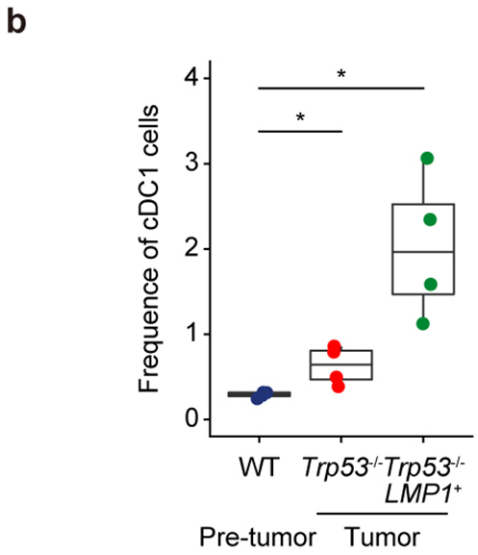


**b,** Proportion of cCD1 cells in SP from WT (at 8 weeks old), *Trp53*$^{-/-}$ (at tumor onset), and *Trp53*$^{-/-}$*LMP1*$^{+}$ (at tumor onset) mice (n = 4 each). Proportion in nonmalignant cells are shown for tumor-bearing mice. *P < 0.05, two-sided Welch's t-test.

**Reviewer #3 (Remarks to the Author):**

The authors have provided additional data demonstrating comparable pathway activation between the TP53 mutated ENKTCL mouse model and human ENKTCL, which enhances the translational potential. There were also some differences observed as expected in the absence of EBV, such as a lack of hypermethylation in the tumor cells from the mouse. There are a few outstanding questions and clarifications that would help in the interpretation of the findings.

We appreciate the reviewer for the time and expertise in reviewing the manuscript and are very pleased that they consider “The authors have provided additional data demonstrating comparable pathway activation between the *TP53* mutated ENKTCL mouse model and human ENKTCL, which enhances the translational potential.”

**#3-1**

The definition of the cell of origin is still somewhat unclear-the authors state that the cell of origin for the murine lymphoma must be an immature NK cell as it is CD122+/Lin-, however this population was later described to also harbor T cell and non-NK ILC potential. In addition, these cells were shown to express Tbet and Eomes, and not NK1.1, yet Tbet and Eomes would normally be expressed after/coinciding with NK1.1 expression in the NK cell lineage. The other antigens evaluated are likewise not specific to NK cells, and there are a mix of immature and mature markers expressed (including KLRG1) which point away from a precursor population. The NK cell development pathway is well characterized in mouse, with numerous reports utilizing reporter mice and/or genetic depletion models in the last few years, and comparing the transcriptional and immunophenotypic findings to what is already established in the field for development would be helpful to defining this population as the current description alone is insufficient to define an NK-restricted precursor population.

We appreciate the reviewer's insightful comments regarding the cell of origin for the mouse NK-cell lymphoma. In general, the cell-of-origin of lymphomas is estimated by identifying a normal counterpart showing a similar surface marker phenotypes and/or transcriptomic/epigenetic profiles to tumor cells. However, as tumor cells frequently show aberrant expressions of various surface markers and exhibit deregulated activity of transcription factors, it is sometimes difficult to determine the cell-of-origin[8].

In the initial manuscript, we showed that (i) mouse NK-cell tumors are Lin (Gr1, Ter119, CD19, and CD3)$^{-}$CD122$^{+}$NK1.1, resembling immature NK cells (**Fig. 1f**), and (ii) mouse NK-cell tumors showed a marked increase of KLRG1 expression compared to normal NK cells (**Fig. 6a,b**). In the first revision, to address the reviewer’s concern, we performed flow cytometric analysis of additional NK-cell transcription factors and

surface markers (**Fig. 1h and Supplementary Fig. 1d**). In this revision, to enable direct comparisons between the murine NK-cell tumors and normal NK cells at various stages of differentiation (as detailed in #3-4), we have added new control data by assessing Eomes and T-bet expressions by intracellular flow cytometry (**Fig. 1h**) and surface marker expressions by flow cytometry (**Supplementary Fig. 1d**) in $Lin^-CD122^+NK1.1^-$ and $Lin^-CD122^+NK1.1^+$ cells in the SG and SP from WT mice using the same methods. As a result, we found that mouse NK-cell tumors had high expressions of NK-cell transcription factors (Eomes and T-bet), variable expressions of lineage-committed NK-cell markers (CD43, CD146 [MCAM], CD226 [DNAM1], and Ly6C), but no or almost no expression of CD11b and CD62L (**Fig. 1h and Supplementary Fig. 1d**).

High expressions of Eomes and T-bet in mouse NK-cell tumors are consistent with a recent report showing high expressions of Eomes and T-bet in human ENKTCL samples[9]. Together with the absence of several NK-cell maturation markers (namely NK1.1 and CD11b), a high T-bet expression suggests immature NK cells as the cell-of-origin, given that T-bet is expressed from NK-cell progenitors and indispensable for the transition from NK-cell progenitors to immature NK cells[10]. By contrast, Eomes is expressed in mature NK cells and essential for the development of mature NK cells[10]. Together with the expression of KLRG1, a differentiation and senescence marker of NK cells, a high Eomes expression suggests mature NK cells as the cell-of-origin, although we believe that KLRG1 was aberrantly expressed in mouse NK-cell tumors. These results suggest that it is difficult to determine which NK-cell maturation stage mouse NK-cell tumors resemble based on the expressions of transcription factors and surface markers.

We showed that *Trp53*$^{-/-}$ mice exhibited increased immature ($Lin^-CD122^+NK1.1^-$) NK cells and decreased mature ($Lin^-CD122^+NK1.1^+CD11b^+$) NK cells in the SG, while there was no difference in the frequency of NK-cell subpopulations in the SP and BM between WT and *Trp53*$^{-/-}$ mice (**Fig. 2a and Supplementary Fig. 2c**). This is the main reason why immature NK cells are considered as the cell-of-origin. In addition, this interpretation is consistent with a recent study showing that ENKTCL cells exhibit a similar surface immunophenotype and DNA methylation signature to NK-cell developmental intermediates present in the tonsils and/or peripheral blood, thereby suggesting that ENKTCL cells are arrested at earlier stages of NK-cell maturation[9].

Given that it is difficult to determine which NK-cell maturation stage mouse NK-cell tumors resemble based on the expressions of transcription factors and surface markers, we have decided to weaken the statement regarding the interpretation of the expression of NK-cell transcription factors and surface markers in **Results** and have added the explanation and the data in **Discussion, Fig. 1h**, **and Supplementary Fig. 1d** in the revised manuscript as follows.

**Results**

**(Page 6, line 129)**

These cells also expressed NK-cell transcription factors (such as Eomes and T-bet), consistent with a recent report analyzing human ENKTCL[13]. They also showed variable expressions of lineage-committed NK-cell markers (such as CD43, CD146 [MCAM], CD226 [DNAM1], and Ly6C), but had no or almost no expressions of CD62L and CD11b (**Fig. 1h and Supplementary Fig. 1d**)~~, resembling immature NK cells within the lineage-committed NK-cell compartment~~.

**Discussion**

**(Page 15, line 345)**

Differential effects of *Trp53* loss on tissue-resident NK cells at the pre-tumor stage and high expression of tissue-resident markers in mouse and human NK-cell tumors suggest that tissue-resident NK cells are a putative cell-of-origin of ENKTCL. Among NK-cell transcription factors, T-bet is expressed from NK-cell progenitors and indispensable for the transition from NK-cell progenitors to immature NK cells, while Eomes, together with maturation markers (such as NK1.1 and CD11b), is expressed in mature NK cells and essential for the development of mature NK cells[18]. Therefore, it is difficult to determine which NK-cell maturation stage mouse NK-cell tumors resemble, but *Trp53*-mediated immature NK-cell expansion at the pre-tumor stage implies that these cells are responsible for ENKTCL development. Our findings align with and complement a recent study showing that ENKTCL cells exhibit a similar surface immunophenotype and DNA methylation signature to NK-cell developmental intermediates present in the tonsils and/or peripheral blood, thereby suggesting that ENKTCL cells are arrested at earlier stages of NK-cell maturation[13].

**Fig. 1h**

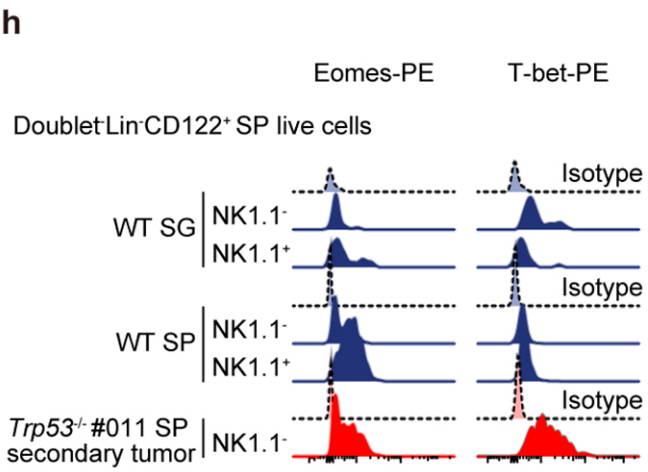


**h,** Representative histograms of Eomes and T-bet expression in Lin⁻CD122⁺NK1.1⁻ and Lin⁻CD122⁺NK1.1⁺ cells in SG and SP from WT mice (at 8 weeks old) and *Trp53*$^{-/-}$ secondary tumors in SP. Isotype controls are shown as shaded histograms.

**Supplementary Fig. 1d**

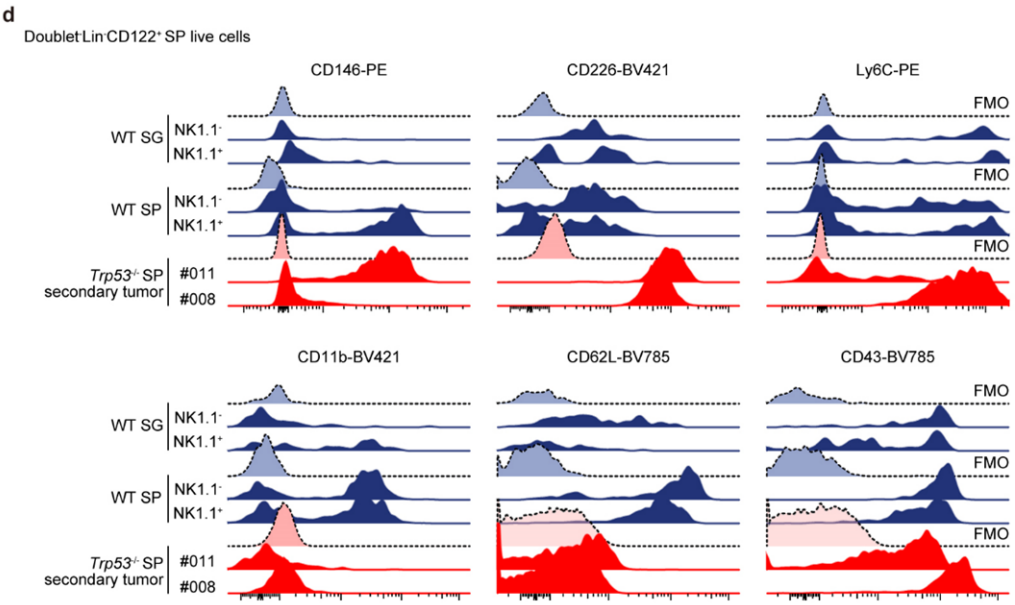


**d,** Representative histograms of CD146, CD226, Ly6C, CD11b, CD62L, and CD43 expression in Lin⁻CD122⁺NK1.1⁻ and Lin⁻CD122⁺NK1.1⁺ cells in SG and SP from WT mice (at 8 weeks old) and *Trp53*$^{-/-}$ secondary tumors in SP. Fluorescence minus one (FMO) controls are shown as shaded histograms.

**#3-2**

The authors also stated this is the first report defining the cell of origin being a tissue residency NK cell, however recent reports on human NK lymphoma have already established the association between tissue resident NK cell phenotypes and categories of NK lymphoma (reference #13). Discussing the findings in this model with the established human data would increase the relevancy/translation. In addition, CD49a alone does not demonstrate tissue residency as CD49a is well established as being upregulated on activated NK cells.

We appreciate the reviewer's comment. Indeed, Mundy-Bosse et al. investigated how ENKTCL ontogeny relates to normal NK-cell development using immunophenotypic and epigenetic analyses. Specifically, they demonstrated that ENKTCL cells exhibit a surface immunophenotype similar to stage 4a (= immature) NK-cell developmental intermediates (NKDI) found in the tonsils based on CD16 and NKp80 expressions. In addition, they generated genome-wide DNA methylation profiles using FFPE samples of ENKTCL with Infinium Methylation EPIC array and compared the profiles with normal tonsil- and blood-derived NKDIs. They found that ENKTCL samples showed a similar methylation signature to stage 4 (immature) and 5 (mature) NKDIs present in the peripheral blood and/or tonsils. Based on these results, they argued that neoplastic NK cells are arrested at earlier stages of NK-cell maturation.

In this study, we have pointed to tissue-resident NK cells as the cell-of-origin of ENKTCL because (i) At the pre-tumor stage, *Trp53* deletion-mediated phenotypic and gene expression changes were exclusively detected in SG NK cells, which are predominantly tissue-resident, but not in SP or BM NK cells, which are mainly conventional NK cells (**Fig.2 and Supplementary Fig.2**); (ii) mouse NK-cell tumors showed highly expressed tissue-resident markers, such as CD69 and CD49a (**Fig. 2e**); (iii) GSEA analysis of human ENKTCL RNA-seq data revealed upregulation of a tissue-resident NK-cell signature and downregulation of a circulating NK-cell signature in ENKTCL tumors (**Fig. 2f, Supplementary Fig. 2j, and Supplementary Table 4**); and (iv) Immunohistochemical analysis showed high expression of CD49a in human ENKTCL (**Fig. 2g**). Thus, our findings in these murine models indeed align with and further extend the human data presented by Mundy-Bosse et al, collectively providing evidence that ENKTCL originates from tissue-resident NK cells.

As the reviewer pointed out, CD49a alone does not mean tissue residency. Thus, we have suggested tissue-resident NK cells as their cell-of-origin of ENKTCL based on all of the above reasons.

Therefore, as the reviewer suggested, we have added the explanation in **Discussion** in the revised manuscript as follows.

**Discussion**

**(Page 15, line 345)**

Differential effects of *Trp53* loss on tissue-resident NK cells at the pre-tumor stage and high expression of tissue-resident markers in mouse and human NK-cell tumors suggest that tissue-resident NK cells are a putative cell-of-origin of ENKTCL. Among NK-cell transcription factors, T-bet is expressed from NK-cell progenitors and indispensable for the transition from NK-cell progenitors to immature NK cells, while Eomes, together with maturation markers (such as NK1.1 and CD11b), is expressed in mature NK cells and essential for the development of mature NK cells[18]. Therefore, it is difficult to determine which NK-cell maturation stage mouse NK-cell tumors resemble, but *Trp53*-mediated immature NK-cell expansion at the pre-tumor stage implies that these cells are responsible for ENKTCL development. Our findings align with and complement a recent study showing that ENKTCL cells exhibit a similar surface immunophenotype and DNA methylation signature to NK-cell developmental intermediates present in the tonsils and/or peripheral blood, thereby suggesting that ENKTCL cells are arrested at earlier stages of NK-cell maturation[13].

**#3-3**

The new Cibersort data from primary ENKTCL did not specify the mutational profile of those samples-was there myeloid infiltration observed in TP53 mutated human ENKTCL? It was also curious that only a low proportion of NK cell infiltration was shown for some of the sequencing samples-wouldn't the vast majority of the tumor samples be associated with an NK cell transcriptional profile if the sample was primarily of tumor origin? Was there any normal adjacent tissue or control tissue that was analyzed in the same manner to provide background immune cell composition?

We appreciate the reviewer's insightful comments and questions. We demonstrated that (i) EBV-encoded latent membrane protein 1 (LMP1) expression caused diverse microenvironmental changes, particularly myeloid expansion in mouse models (**Fig. 4c,d**); and (ii) deconvolution of RNA-seq data of human ENKTCL revealed that myeloid cell infiltration was observed in all tumors (**Supplementary Fig. 5g,h**). Thus, myeloid cell infiltration was observed in *TP53*-mutated samples, although this observation was not limited to *TP53*-mutated samples. As the reviewer suggested, we have highlighted *TP53*-mutated samples in red in the results of CIBERSORTx deconvolution (**Supplementary Fig. 5g**) for clarity.

We performed CIBERSORTx deconvolution to show that myeloid cell infiltration was observed in human ENKTCL samples (**Supplementary Fig. 5g**), which complements the results of immunohistochemical analysis validating the presence of

CD11c$^{+}$ DC in the tumor microenvironment of human ENKTCL (**Supplementary Fig. 6j**). Thus, we would like to make sure that the aim of this analysis was not to evaluate the tumor content in human ENKTCL.

To address the reviewer's concern regarding a low proportion of NK cells in human ENKTCL samples, we first analyzed publicly available RNA-seq data of two human ENKTCL cell lines, KHYG-1 and MTA, using CIBERSORTx, and found that these cell lines showed various proportions of T and NK cells (**Reviewer-only Fig. 1**), although they are a clonal NK-cell or T-cell line. These results suggest that it is difficult to evaluate the proportion of not only tumor cells but also normal T and NK cells using CIBERSORTx in human ENKTCL samples. Together with a frequent low tumor content of human ENKTCL samples, as shown by several genetic studies[11-13], these observations can explain the reviewer's concern.

Given discriminating tumor cells and normal T and NK cells is difficult in CIBERSORTx deconvolution of human ENKTCL samples, we analyzed these results again by evaluating the proportion of myeloid cells in nonmalignant cells after excluding T and NK cells. At this point, as the reviewer suggested, we have also analyzed publicly available RNA-seq data (SRP351297) from matched normal tonsils obtained from ENKTCL patients[14]. As a result, we have found that myeloid cells are increased in human ENKTCL compared to normal tonsils (**Supplementary Fig. 5g, h**). In addition, the public RNA-seq data we analyzed (SRP351297) also included those of tumor samples from the same ENKTCL patients. Consequently, we reanalyzed human ENKTCL RNA-seq data, including these 3 additional ENKTCL samples (41 samples in total), and obtained similar results to those in the previous manuscript (**Fig. 2f, 5g, 6d, Supplementary Fig. 2i,j, 3g, 5g, and 6h,i, and Supplementary tables 3 and 10**).

Therefore, we have added the explanation and the data in **Results and Supplementary Fig. 5g,h**, and revised the data in **Fig. 2f, 5g, 6d, Supplementary Fig. 2i,j, 3g, 5g, and 6h,i, and Supplementary tables 3 and 10** in the revised manuscript as follows.

**Results**

**(Page 10, line 239)**

In addition, deconvolution of RNA-seq data of human ENKTCL revealed that myeloid cell infiltration was observed in all tumors, with significantly higher proportions compared with normal tonsils (**Supplementary Fig. 5g,h and Supplementary Table 10**).

**Reviewer-only Fig. 1**

**[figure redacted]**

CIBERSORTx deconvolution of RNA-seq data of two human ENKTCL cell lines, KHYG-1 and MTA are shown.

**Supplementary Fig. 5g**

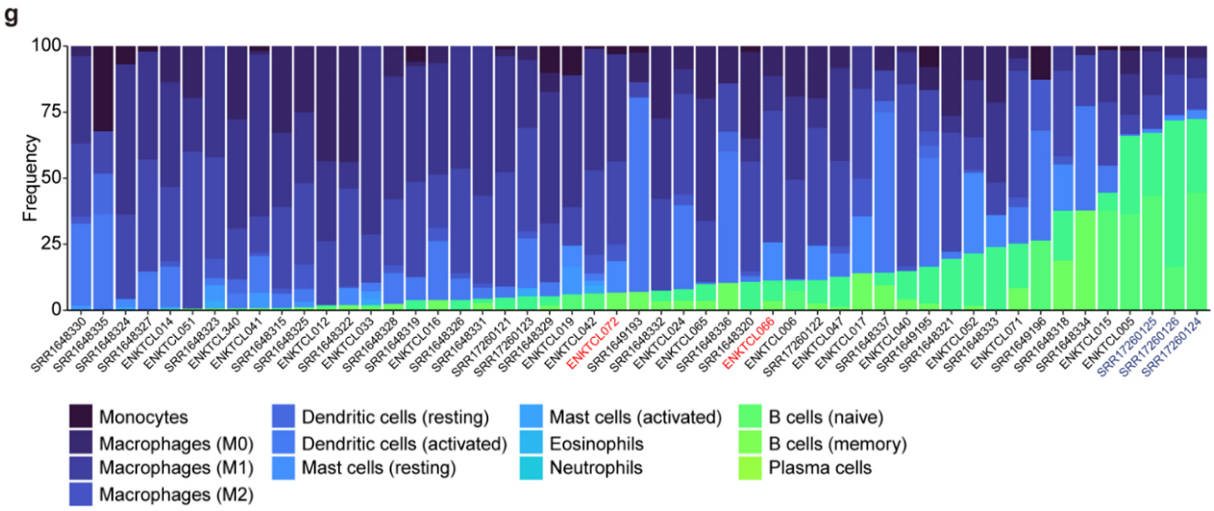


**g,** CIBERSORTx deconvolution of RNA-seq data of 41 human ENKTCL tumors and 3 normal tonsils. Proportion in nonmalignant cells (after excluding T and NK cells) are shown. Normal tonsils and *TP53*-mutated tumors are colored in blue and red, respectively.

**Supplementary Fig. 5h**

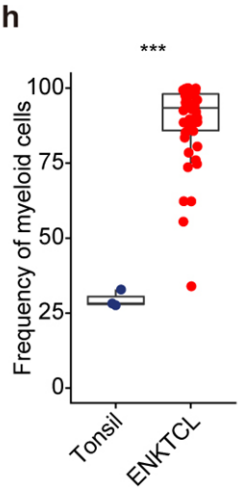


**h,** Proportion of myeloid cells (after excluding T and NK cells) in 41 human ENKTCL tumors and 3 normal tonsils. ***P < 0.0005, two-sided Welch's t-test.

**Methods**

**(Page 36, line 714) Bulk RNA-seq and analysis**

Publicly available RNA-seq data for 20 ENKTCL tumors and 3 normal tonsils from ENKTCL patients and 1 normal NK cell from healthy donor (accession number SRP351297[36] and SRA2008200[37]) were also obtained from the National Center for Biotechnology Information Sequence Read Archive.

**(Page 36, line 721) Bulk RNA-seq and analysis**

Batch effect among datasets was corrected using ComBat function in the R package sva (version 3.42.0), while preserving cell type-specific effects[38]. Adjusted expression values below zero were subsequently set to zero.

**(Page 37, line 742) Immune cell deconvolution using CIBERSORTx**

As discriminating tumor cells and normal T and NK cells is difficult, proportion in nonmalignant cells was estimated after excluding T and NK cells.

**#3-4**

There is an overall lack of controls being pictured in the new data (and explanation for what is being shown). In the flow histogram plots for example, is that an isotype control being shown, or an internal negative? How do these levels compare to those found in stages of murine NK cells (for the transcription factor data)? Please describe in more detail.

We appreciate the reviewer's concern regarding the controls and their presentation in our data. We had already added the controls in **Fig. 1h** and **Supplementary Fig. 1d** in the first revision, but we apologize that they had not been clearly indicated. Indeed, isotype controls were used for evaluating Eomes and T-bet expressions in **Fig. 1h** and fluorescence minus one (FMO) controls were used for evaluating surface marker expressions in **Supplementary Fig. 1d**. In **Supplementary Fig. 6f** (added in this revision), isotype controls were used for evaluating IFN-γ expression. We clearly stated these in the revised manuscript as follows.

As detailed in #3-1, we have added new control data by assessing Eomes and T-bet expressions by intracellular flow cytometry (**Fig. 1h**) and surface marker expressions by flow cytometry (**Supplementary Fig. 1d**.) in $Lin^-CD122^+NK1.1^-$ and $Lin^-CD122^+NK1.1^+$ cells in SG and SP from WT mice using the same methods. These experiments provide a more comprehensive set of control data, allowing us for direct comparisons between the murine NK-cell tumors and normal NK cells at various stages of differentiation.

Therefore, we have clearly explained about the controls in **Fig. 1h**, **Supplementary Fig. 1d and 6f, and Methods** and added the new control data in **Fig. 1h and Supplementary Fig. 1d** in the revised manuscript as follows.

**Results**

**(Page 6, line 129)**

These cells also expressed NK-cell transcription factors (such as Eomes and T-bet), consistent with a recent report analyzing human ENKTCL[13]. They also showed variable expressions of lineage-committed NK-cell markers (such as CD43, CD146 [MCAM], CD226 [DNAM1], and Ly6C), but had no or almost no expressions of CD62L and CD11b (**Fig. 1h and Supplementary Fig. 1d**)~~, resembling immature NK cells within the lineage-committed NK-cell compartment~~.

**Fig. 1h**

**h**

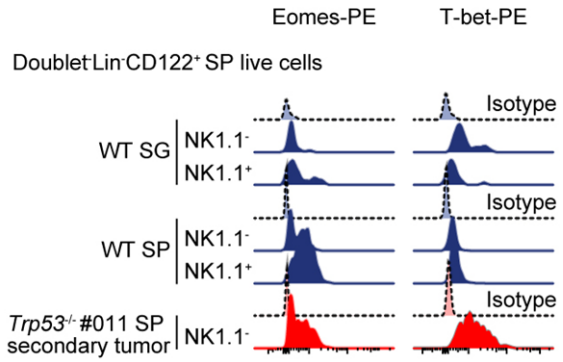


**h,** Representative histograms of Eomes and T-bet expression in Lin$^-$CD122$^+$NK1.1$^-$ and Lin$^-$CD122$^+$NK1.1$^+$ cells in SG and SP from WT mice (at 8 weeks old) and *Trp53*$^{-/-}$ secondary tumors in SP. Isotype controls are shown as shaded histograms.

## Supplementary Fig. 1d

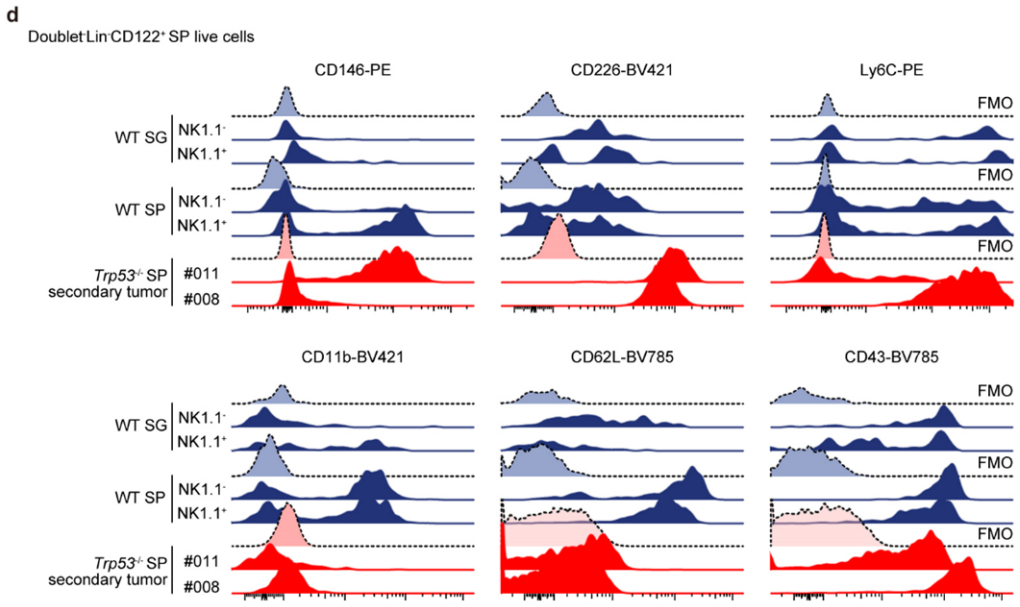


**d,** Representative histograms of CD146, CD226, Ly6C, CD11b, CD62L, and CD43 expression in Lin$^-$CD122$^+$NK1.1$^-$ and Lin$^-$CD122$^+$NK1.1$^+$ cells in SG and SP from WT mice (at 8 weeks old) and *Trp53*$^{-/-}$ secondary tumors in SP. Fluorescence minus one (FMO) controls are shown as shaded histograms.

## Supplementary Fig. 6f

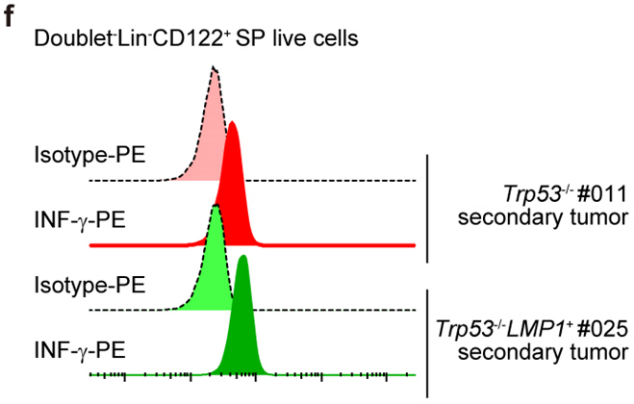


**f,** Representative histograms of IFN-γ expressions in Lin$^-$CD122$^+$ cells from *Trp53*$^{-/-}$ and *Trp53*$^{-/-}$*LMP1*$^+$ tumors. Isotype controls are shown as shaded histograms.

## Methods

**(Page 32, line 611) Flow cytometry**

Isotype controls were used for intracellular flow cytometry, while fluorescence minus one (FMO) controls were used for all other flow cytometric analyses.

**#3-5**

For histology, please provide normal tissue staining to demonstrate specificity of the antibody staining being evaluated. H+E was provided for mouse, but the antibody staining should likewise have controls.

We appreciate the reviewer's suggestion. To demonstrate the specificity of our antibody staining, we performed immunohistochemical analysis on human diffuse large B-cell lymphoma samples using the same antibodies (CD49a, CXCR6, CXCR3, and KLRG1) and protocols as used for the ENKTCL specimens and confirmed negative expressions of these surface proteins in DLBCL tumor cells (**Supplementary Fig. 8**). In addition, we have performed hematoxylin and eosin staining for human ENKTCL samples (**Supplementary Fig. 2k**). Therefore, we have added the data in **Supplementary Fig. 2k and 8 and Methods** in the revised manuscript as follows.

**Supplementary Fig. 2k**

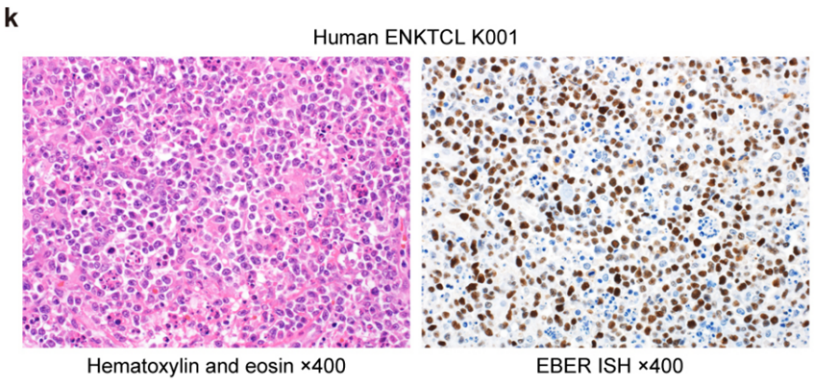


**k,** Representative image of hematoxylin and eosin staining (left) and EBV-encoded small RNA (EBER) in situ hybridization (right) in a human ENKTCL sample.

**Supplementary Fig. 8. Validation of the specificity of the antibodies used in Immunohistochemical analysis.**

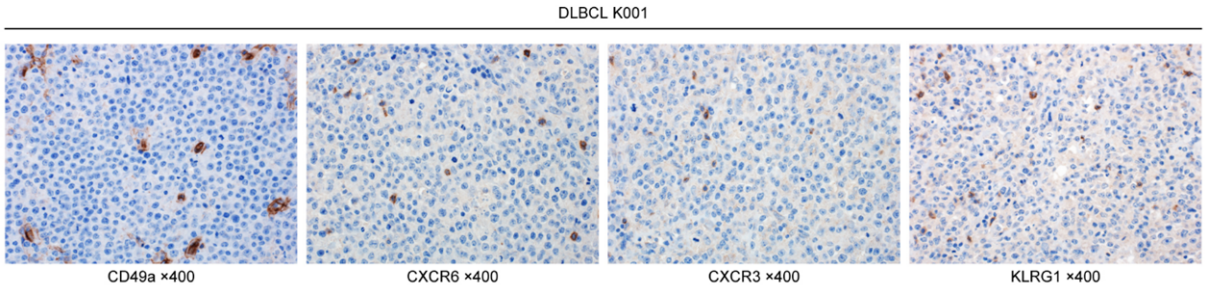


Representative images of CD49a, CXCR6, CXCR3, and KLRG1 immunostaining in a human diffuse large B-cell lymphoma (DLBCL) sample.

**Methods**

**(Page 32, line 600) Histology**

Human diffuse large B-cell lymphoma samples were used to confirm the specificity of the antibodies (**Supplementary Fig. 8**).

**#3-6**

Flow dot plots should be shown for the new IFNγ data in addition to bar graph (along with isotype controls)

As the reviewer suggested, we have added a representative histogram of intracellular flow cytometry data showing IFN-γ expressions in $Lin^{-}CD122^{+}$ cells from *Trp53*$^{-/-}$ and *Trp53*$^{-/-}$*LMP1*$^{+}$ tumors together with isotype controls in **Supplementary Fig. 6f** in the revised manuscript as follows.

**Supplementary Fig. 6f**

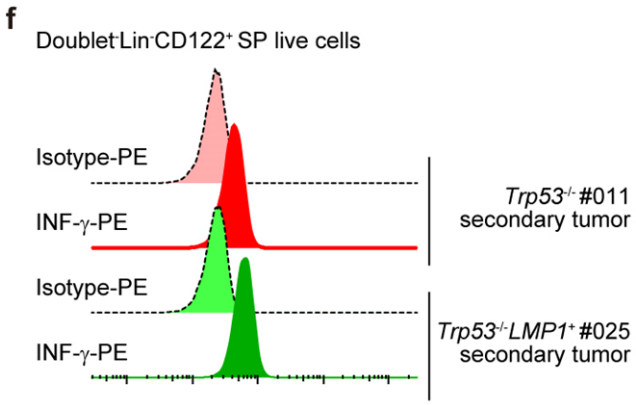


**f,** Representative histograms of IFN-γ expressions in Lin⁻CD122⁺ cells from *Trp53*$^{-/-}$ and *Trp53*$^{-/-}$*LMP1*$^{+}$ tumors. Isotype controls are shown as shaded histograms.

## References


1 Wang, H. *et al.* The transcription factor Foxp1 is a critical negative regulator of the differentiation of follicular helper T cells. *Nat Immunol* **15**, 667-675 (2014). https://doi.org/10.1038/ni.2890

2 Böttcher, J. P. *et al.* Functional classification of memory CD8(+) T cells by CX3CR1 expression. *Nat Commun* **6**, 8306 (2015). https://doi.org/10.1038/ncomms9306

3 Hayward, S. L. *et al.* Environmental cues regulate epigenetic reprogramming of airway-resident memory CD8(+) T cells. *Nat Immunol* **21**, 309-320 (2020). https://doi.org/10.1038/s41590-019-0584-x

4 Vanneste, D. *et al.* MafB-restricted local monocyte proliferation precedes lung interstitial macrophage differentiation. *Nat Immunol* **24**, 827-840 (2023). https://doi.org/10.1038/s41590-023-01468-3

5 Luber, C. A. *et al.* Quantitative proteomics reveals subset-specific viral recognition in dendritic cells. *Immunity* **32**, 279-289 (2010). https://doi.org/10.1016/j.immuni.2010.01.013

6 Xue, R. *et al.* Liver tumour immune microenvironment subtypes and neutrophil heterogeneity. *Nature* **612**, 141-147 (2022). https://doi.org/10.1038/s41586-022-05400-x

7 Liu, L. *et al.* Single cell sequencing reveals that CD39 inhibition mediates changes to the tumor microenvironment. *Nat Commun* **13**, 6740 (2022). https://doi.org/10.1038/s41467-022-34495-z

8 Shaffer, A. L., 3rd, Young, R. M. & Staudt, L. M. Pathogenesis of human B cell lymphomas. *Annu Rev Immunol* **30**, 565-610 (2012). https://doi.org/10.1146/annurev-immunol-020711-075027

9 Mundy-Bosse, B. L. *et al.* Identification and Targeting of the Developmental Blockade in Extranodal Natural Killer/T-cell Lymphoma. *Blood Cancer Discov* **3**, 154-169 (2022). https://doi.org/10.1158/2643-3230.BCD-21-0098

10 Gordon, S. M. *et al.* The transcription factors T-bet and Eomes control key checkpoints of natural killer cell maturation. *Immunity* **36**, 55-67 (2012). https://doi.org/10.1016/j.immuni.2011.11.016

11 Kataoka, K. *et al.* Frequent structural variations involving programmed death ligands in Epstein-Barr virus-associated lymphomas. *Leukemia* **33**, 1687-1699 (2019). https://doi.org/10.1038/s41375-019-0380-5

12 Ito, Y. *et al.* Comprehensive genetic profiling reveals frequent alterations of driver genes on the X chromosome in extranodal NK/T-cell lymphoma. *Cancer Res* (2024). https://doi.org/10.1158/0008-5472.Can-24-0132

13 Dong, G. *et al.* Genomic profiling identifies distinct genetic subtypes in extra-nodal natural killer/T-cell lymphoma. *Leukemia* **36**, 2064-2075 (2022). https://doi.org/10.1038/s41375-022-01623-z

14 Zhou, J. *et al.* Super-enhancer-driven TOX2 mediates oncogenesis in Natural Killer/T Cell Lymphoma. *Mol Cancer* **22**, 69 (2023). https://doi.org/10.1186/s12943-023-01767-1